FINITE ELEMENT ANALYSIS OF LOCALISED FAULT IN DEEP GROOVE BALL BEARING

A THESIS SUBMITTED IN PARTIAL FULFILLMENT OF THE REQUIREMENT FOR THE AWARD OF THE DEGREE OF

MASTER OF TECHNOLOGY
(COMPUTATIONAL DESIGN)
TO

DELHI TECHNOLOGICAL UNIVERSITY

SUBMITTED BY
YAMAL SINGH

ROLL NO. - 2K15/CDN/15

UNDER THE GUIDANCE OF

MR. PARAS KUMAR
ASSISTANT PROFESSOR

DELHI TECHNOLOGICAL UNIVERSITY

DEPARTMENT OF MECHANICAL, PRODUCTION & INDUSTRIAL AND AUTOMOBILE ENGINEERING
DELHI TECHNOLOGICAL UNIVERSITY
BAWANA ROAD, DELHI-110042
2017

DELHI TECHNOLOGICAL UNIVERSITY

(Formerly Delhi College of Engineering)

Shahbad Daulatpur, Bawana Road,

Delhi-110042

DECLARATION

I, **Yamal Singh (2k15/CDN/15),** hereby certify that the work which is being presented in this thesis entitled **"Finite element analysis of localised fault in deep groove ball bearing"** is submitted in the partial fulfilment of the requirement for degree of **Master of Technology (Computational Design)** in Department of Mechanical Engineering at **Delhi Technological University** is an authentic record of my own work carried out under the supervision of **Mr. Paras Kumar.** The matter embodied in this thesis has not been submitted in any other University/Institute for the award of Master of Technology/certificate. Also, it has not been directly copied from any source without giving its proper reference.

Signature of Student

DELHI TECHNOLOGICAL UNIVERSITY

(Formerly Delhi College of Engineering)

Shahbad Daulatpur, Bawana Road,

Delhi-110042

CERTIFICATE

This is to certify that this thesis report titled **"Finite Element Analysis of Localised Fault in Deep Groove Ball bearing"** being submitted by **Yamal Singh (2k14/CDN/15)** at Delhi Technological University for award of Degree of master of technology as per academic curriculum. It is record of bonafide research work carried out by the student for partial fulfilment of the requirement for the award of Master of Technology degree in Computational Design. The work is original has not been submitted earlier in full or part of any purpose before.

Mr. Paras Kumar

Assistant Professor

Mechanical Engineering Department

Delhi Technological University

Delhi-110042

ACKNOWLEDGEMENTS

First and foremost, praises and thanks to the God, the Almighty, for his showers of blessings throughout my research work to complete the research successfully.

I would like to extend my gratitude to **Prof. R. S. Mishra, Head,** Department of Mechanical Engineering, Delhi Technological University, for providing this opportunity to carry out the present thesis work.

I would like to express my deep and sincere gratitude to my research supervisor, **Mr. Paras Kumar,** Department of Mechanical Engineering, Delhi Technological University, for giving me the opportunity to do research and providing invaluable guidance throughout this research. His dynamism, vision, sincerity and motivation have deeply inspired me. He has taught me the methodology to carry out the research and to present the research works as clearly as possible. It was a great privilege and honour to work and study under his guidance. I am extremely grateful for what he has offered me. I want to extend gratitude to **Prof. Vikas Rastogi** for providing me the facilities of design centre to work on my major project.

I am also grateful to all the faculty members of the Mechanical Engineering Department for moulding me at correct time so that I can have a touch at final destination and to all my friends, for the help, moral support and encouragement; they had given to me during completion of dissertation work.

I am extremely grateful to my parents and family for their love, prayers, caring and sacrifices for educating and preparing me for my future.

Yamal Singh

M. Tech. (COMPUTATIONAL DESIGN)
2K15/CDN/15

ABSTRACT

Rolling element bearings as an important component in almost all types of rotating machines have been wide spreadly used and its failure is one of the foremost causes of failure and breakdowns in rotating machinery, resulting in significant economic loss. It is highly imperative to investigate the failure causes in order to improve the design and operating conditions to bear with the decreasing overall efficiency and economics involved.

In present age many industries benefit from the use of deep groove ball bearings like, Agricultural, food processing, machine tool, material handling, medical / pharmaceutical and wind energy etc. Deep groove ball bearings are versatile as they can carry radial and axial loads, they have a wider range of applications for many industries and they lead to cost savings because they create less friction torque, this lowers operating temperature (which extends the life of the bearing) and reduces energy cost of running equipment (such as conveyor belts). Require less upkeep because of their simple design, low operating temperature, and low friction, deep groove ball bearings have a longer expected shelf life than other bearings. They do not require additional lubrication after installation, which also means less maintenance downtime. But due to mishandling, environmental effects and failure in operational conditions there is development of localized and distributed defects over the time, which lead to lead to seizing of machinery gradually that leads to down time. From practical conditional monitoring to FEA and dynamic models have been developed for these defects in ball bearing and thus to minimize the detrimental effects associated.

Finite element analysis is used to model the localised faults in inner race of deep groove ball bearing. Ansys workbench's transient module is used to simulate the impact over the defect and nodal parameters are captured to understand the severity of vibrations generated by the defects upon interaction with the balls in one contact simulation. The feasibility of FEA is also established for the modelling of faults in ball bearing and simplistic approach for most convenient way of simulating such

defects have been developed for further studies in this field. The project focuses on procedural detailing and using apt solvers to arrive to most time efficient simulation technique. Dynamics of the system is very well projected by the transient model of faulted ball bearing.

Emphasis is laid on analysing the impact of varying sizes of the faults on the severity of vibrations created upon interaction of ball over the defect on the inner race for single pass. Comparative study between cylindrical and square faults of same longitudinal and lateral sizes have been done to implicate their detrimental effects on the operation of the faulted deep grove ball bearing. Simulation results show that as defect size increases the severity of vibration increase drastically and rectangular defects prove to produce much adverse effects as compared to cylindrical defects. Further research avenues for modelling and simulation of faults in bearing have been suggested.

Key words: Finite element analysis, Ansys work bench, Transient model, localised faults.

Table of Contents

TABLE OF FIGURES

LIST OF TABLES

CHAPTER 1: INTRODUCTION

Rolling Element Bearings (REB) are the most common machine elements used in rotating machinery and their failure is the foremost cause of down time in plant machinery. Commonly occurring REB defects are cracks and pits located at outer race, inner race and on the rolling element. These defects generate a sequence of impacts with each passage of rolling element over the defect due to the metal to metal contact.

Rolling element bearings are classified basically into roller bearings and ball bearings and there are further sub divisions. Deep groove ball bearing is widely used ball bearing and are very versatile in carrying loads i.e. can handle both axial and radial loads. It has very low coefficient of friction and thereby producing low frictional torque which minimizes the losses and keeps the operating temperature low. Manufacturing process is also very simple and cheap because of its easy geometry. But despite of all advantages bearings often faces with challenge of development of localised and distributed defects which induce heavy vibrations in the operation of the machinery. These defects generate a sequence of impacts with each passage of rolling element over the defect due to the metal to metal contact. There is sudden decrease in life of bearing and the other components also face chances of damage, which incurs huge down time for the machinery. In practice, it is quite difficult to obtain vibration signal from bearing having incipient defects; thus, many researchers have attempted to simulate the vibration signal emanating from bearing having incipient fault. In the present work, a method to simulate the ball bearing having an incipient crack on inner race has been presented. Transient analysis of the finite element model of faulted deep groove ball bearing is performed and nodal parameters like velocity, acceleration, of a node on a region on inner race that is not constrained was recorded with respect to time. Square and cylindrical shapes of localised defects on the inner race is modelled and the size is varied to study the impact of size of the faults on vibrations induced. Comparative analysis of different shape of defects is also done.

1.1. Rolling element bearing construction

In Rolling bearing construction, most rolling bearings consist of rings with raceway (inner ring and outer ring), rolling elements (either balls or rollers) and cage. The cage separates the rolling elements at regular intervals, holds them in place within the inner and outer raceways, and allows them to rotate freely.

1.1.2 Raceway (inner ring and outer ring) or raceway washer

The surface on which rolling elements roll is called the "raceway surface". The load placed on the bearing is supported by this contact surface. Generally, the inner ring fits on the axle or shaft and the outer ring on the housing .The raceway of thrust bearing is called "raceway washer," the inner ring is called the "shaft raceway washer" and the outer ring is called the "housing raceway washer."

1.1.3 Rolling elements

Rolling elements classify in two types: balls and rollers. Rollers come in four types: cylindrical, needle, tapered, and spherical. Balls geometrically contact with the raceway surfaces of the inner and outer rings at "points", while the contact surface of rollers is a "line" contact. Theoretically, rolling bearings are so constructed as to allow the rolling elements to rotate orbitally while also rotating on their own axes at the same time.

1.1.4 Cages

Cages function to maintain rolling elements at a uniform pitch so load is never applied directly to the cage and to prevent the rolling elements from falling out when handling the bearing. Types of cages differ according to way they are manufactured, and include pressed, machined and formed cages.

1.2 Classification of rolling bearings Rolling bearings divide into two main classifications**:**

ball bearings and roller bearings. Ball bearings are classified according to their bearing ring configurations: deep groove type and angular contact type. Roller bearings on the other hand are classified according to the shape of the rollers:

cylindrical, needle, tapered and spherical. Rolling bearings can be further classified according to the direction in which the load is applied; radial bearings carry radial loads and thrust bearings carry axial loads. Other classification methods include: 1) number of rolling rows (single, double, or 4-row), 2) separable and non-separable, in which either the inner ring or the outer ring can be detached. There are also bearings designed for special applications, such as: railway car journal roller bearings, ball screw support bearings, turntable bearings, as well as linear motion bearings (linear ball bearings, linear roller bearings and linear flat roller bearings). Types of rolling bearings are given in.

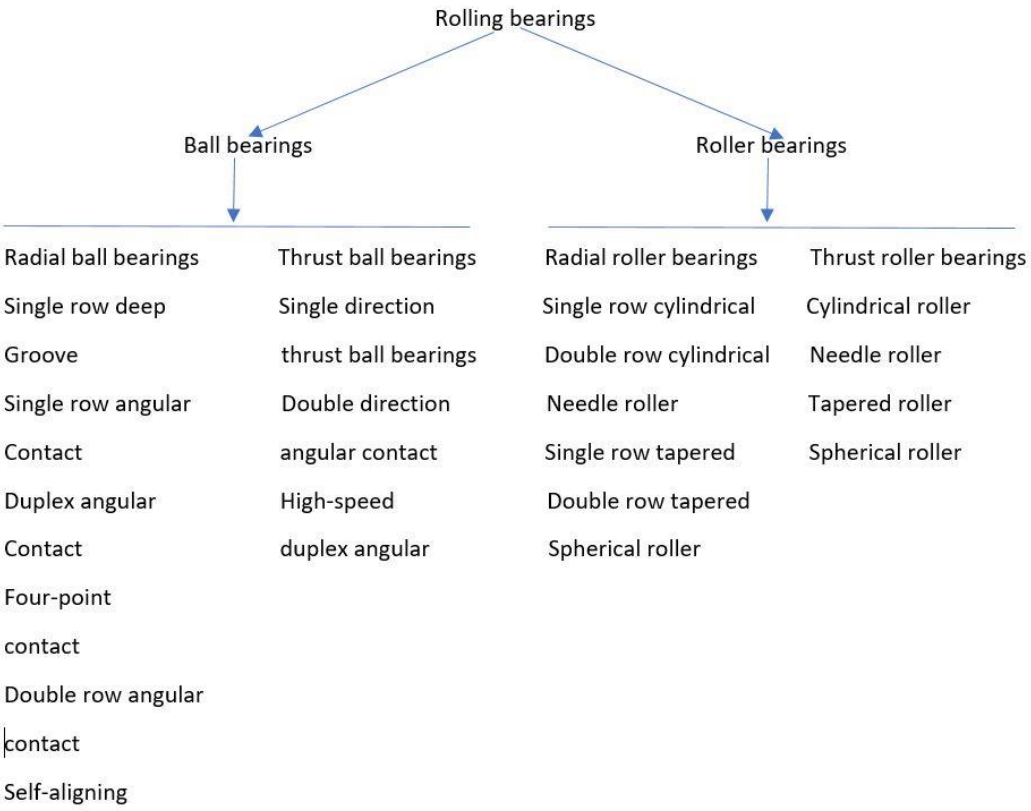

Flow chart 1.1: bearing classification

1.2.2 Characteristics of rolling element bearing

Rolling bearings come in many shapes and varieties, each with its own distinctive features. However, when compared with sliding bearings, rolling bearings all have the following advantages:

- The starting friction coefficient is lower and there is little difference between this and the dynamic friction coefficient.
- They are internationally standardized, interchangeable and readily obtainable.
- They are easy to lubricate and consume less lubricant.
- As a general rule, one bearing can carry both radial and axial loads at the same time.
- May be used in either high or low temperature applications.
- Bearing rigidity can be improved by preloading. Construction, classes, and special features of rolling bearings are fully described in the boundary dimensions and bearing numbering system section.

1.3 Deep groove ball bearing

The most common type of bearing, deep groove ball bearings are widely used in a variety of fields. Deep groove ball bearings include shield bearings and sealed bearings with grease make them easier to use. Deep groove ball bearings also include bearings with a locating snap-ring to facilitate positioning when mounting the outer ring, expansion compensating bearings which absorb dimension variation of the bearing fitting surface due to housing temperature, and TAB bearings that are able to withstand contamination in the lubricating oil.

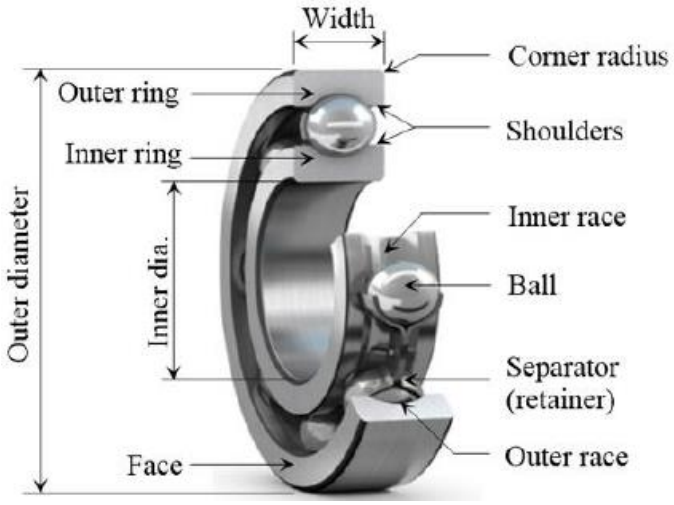

Fig 1.1: Deep groove ball bearing [1]

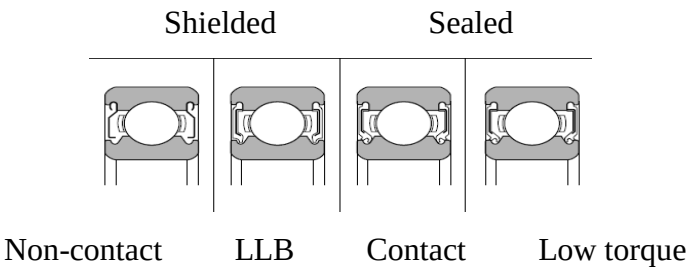

Fig1.2: Configuration of sealed ball bearings [2]

1.3.1 deep groove ball bearing characteristics and advantages

- Deep Groove ball bearings are the most popular of all the ball bearing types because they are available in a wide variety of seal, shield and snap-ring arrangements.
- The bearing ring grooves are circular arcs made slightly larger than the radius of the ball. The balls make point contact with the raceways (elliptical contact when loaded). The inner ring shoulders are of equal height (as the outer ring shoulders).
- Deep Groove ball bearings can sustain radial, axial, or composite loads and because of simple design, this bearing type can be produced to provide both high-running accuracy and high-speed operation.

1.4 Bearing Faults

The bearings act as a source of noise and vibration due to varying compliance as much as the presence of defects in them, which may be classified into distributed and localized defects. The fact that the load distribution on the bearings varies, as the rolling element set rotates round the rings, causes the bearings to behave themselves as a vibration generator. This behaviour may arise as much as from a geometrically perfect bearing as one which possesses imperfections from manufacture, installation, lubrication or inadequate ambient running conditions or some other factor that may help to cause wear or fatigue.

1.4.1 Localized defects

The most common type is the crack of the races or rolling elements, mainly caused when a crack due to fatigue originated sub-superficially is propagated towards the surface until a metal piece is detached causing a small defect. The fault caused by superficial fatigue is accelerated when the bearing is overloaded or submitted to shock or impact loads during their functioning or installation and also with the increase of the rotational speed.

1.4.2 Distributed defects

Within these we find: the surface roughness, waviness, misaligned races and unequal rolling elements. They can be caused by manufacturing errors, inadequate installation or due to wear. The variation of the contact forces between the rolling elements and the races cause an increase in the vibration level. Because it is difficult to discern when the vibration is caused by either distributed or localized defects, it is highly recommended to make an analysis based on; one hand the frequency and, on the other the amplitude of the spectral components

1.4.3 Defects and causes

1.4.3.1. Excessive loads

Usually causes premature fatigue. Can be alleviated by reducing the load or redesigning with a bearing of greater capacity [52].

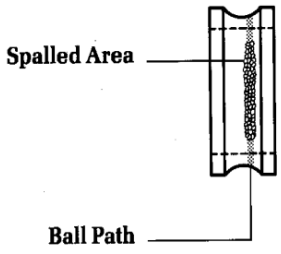

Fig 1.3: Defect due to excessive load [3]

1.4.3.2 Over heating

Symptoms are discoloration of the rings, balls, and cages from gold to blue Temperature in excess of 400° F can anneal the ring and ball materials and degrade or destroy lubricant the resulting loss in hardness reduces the bearing capacity causing early failure in extreme cases, balls and rings will deform.

1.4.3.3 True brinelling

Occurs when loads exceed the elastic limit of the ring material Creates brinell marks which show as indentations in the raceways and increase bearing vibration (noise) Caused by any static overload or severe impact.

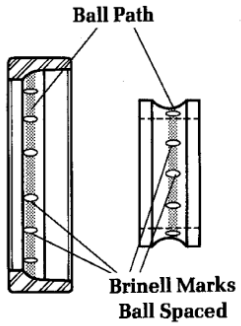

Fig 1.4: Brinelling [3]

1.4.3.4 False brinelling

Creates elliptical wear marks in an axial direction at each ball position with a bright finish and sharp demarcation, often surrounded by a ring of brown debris Indicates excessive external vibration Corrected by isolating bearings from external vibration, and using greases containing anti-wear additives

1.4.3.5 Normal fatigue

failure A fracture of the running surfaces and subsequent removal of small discrete particles of material Also referred to as spalling Can occur on the inner ring, outer ring, or balls A “progressive” failure Once initiated, it will spread with continued operation It will always be accompanied by a marked increase in vibration Remedied by replacing the bearing or redesigning with a bearing that has a greater calculated fatigue life.

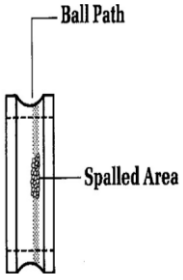

Fig 1.5: Normal fatigue [3]

1.4.3.6 Reverse loading

Angular contact bearings are designed to accept an axial load in one direction only When loaded in the opposite direction, the elliptical contact area on the outer ring is truncated by the low shoulder on that side of the outer ring The result is excessive stress and an increase in temperature, followed by increased vibration and early failure Corrective action is to re-install the bearing correctly.

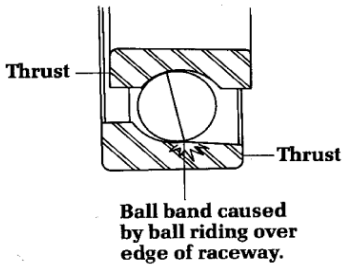

.Figure 1 .6: Lubricant failure [3]

Ball bearings depend on the continuous presence of a very thin (millionths of an inch) film of lubricant between the balls and races, and between the cage, bearing rings, and balls Insufficient or ineffective lubricant results in excessive wear of balls, ring, and cages will that leads to overheating and subsequently catastrophic failure discoloured (blue/brown) ball tracks and balls can occur Failures are typically caused by restricted lubricant flow or excessive temperatures that degrade the lubricant's properties

1.4.3.7 Corrosion

Red/brown areas on balls, race-way, cages, or bands of ball bearings may be present Results from exposing bearings to corrosive fluids or a corrosive atmosphere in extreme cases, can initiate early fatigue failures Corrected by diverting corrosive fluids away from bearing areas and using integrally sealed bearings whenever possible.

1.4.3.8 Misalignment

Can be detected on the raceway of the non-rotating ring by a ball wear path that is not parallel to the raceways edges if it exceeds 0.001 in./in, will cause an abnormal temperature rise in the bearing and/or housing and heavy wear in the cage ball-pockets Appropriate corrective actions include: Inspect shafts and housings for

runout of shoulders and bearing seats Use single point-turned or ground threads on non-hardened shafts and ground threads only on hardened shafts Use precision grade locknuts.

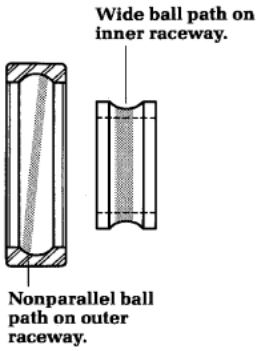

Fig 1.7: Lines due to misalignment [3]

1.4.3.9 Loose fits

Can cause relative motion between mating parts If the relative motion between mating parts is slight but continuous, fretting occurs Fretting is the generation of fine metal particles which oxidize, leaving a distinctive brown color. This material is abrasive and will aggravate the looseness. If the looseness is enough to allow considerable movement of the inner or outer ring, the mounting surfaces (bore, outer diameters, faces) will wear and heat, causing noise and runout problems.

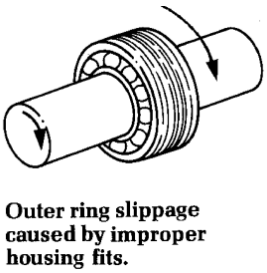

Fig 1.8: Ring slippage [3]

1.4.3.10 Tight fits

Indicated by a heavy ball wear path in the bottom of the raceway around the entire circumference of the inner ring and outer ring Where interference fits exceed the radial clearance at operating temperature, the balls will become excessively loaded, resulting in a rapid temperature rise accompanied by high torque Continued

operation can lead to rapid wear and fatigue Corrective action is a decrease in total interference

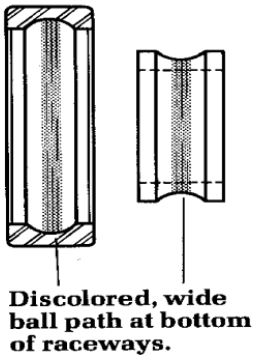

Fig 1.9: Tight fight defect [3]

1.5 Evolution of the fault due to crack

The first symptom that appears when the fault arises, at an early stage, is a vibration with high frequency components due to the generation of stress waves and other kinds, which can excite natural frequencies of housing and races of the bearings or the measuring sensor. In this stage, there is no temperature increase and the cracks are not visible, it is not necessary to change the bearings. In a second stage, the cracks start to be visible and the bearings produce audible sound and in some cases the temperature arises. In this fault stage, spectral components related to fault frequency of bearings in the low and intermediate frequency range appear. These frequencies are commonly named as “characteristic defect frequencies” and they are designed as BPFO (ball pass frequency outer race), BPFI (ball pass frequency inner race), BSF (ball spin frequency) and FTF (fundamental train frequency)[5], depending on the location of the defect; whether it is on the inner race, outer race or on one of the rolling elements. They are determined based upon the geometry and rotational speed of the bearing and can be calculated from simple mathematical expressions or using commercial software. It is necessary in this fault stage to program the change of the bearing. In a third stage, close to a catastrophically failure, the noise increases significantly an overheating may arise, the vibration in the high frequency range decreases, the spectral components of the low frequency range increases and it will be necessary to change the bearing immediately [6]. Although this, the most usual way for it to show when a bearing develops a fault,

each bearing could have different fault modes with a different progression rate, it depends of the load, rotational velocity and lubrication conditions mainly.

1.6 Bearing Frequencies

The five basic motions of the rolling element bearing and their corresponding frequencies are depicted in Fig. 1.9. Most significant frequencies are:

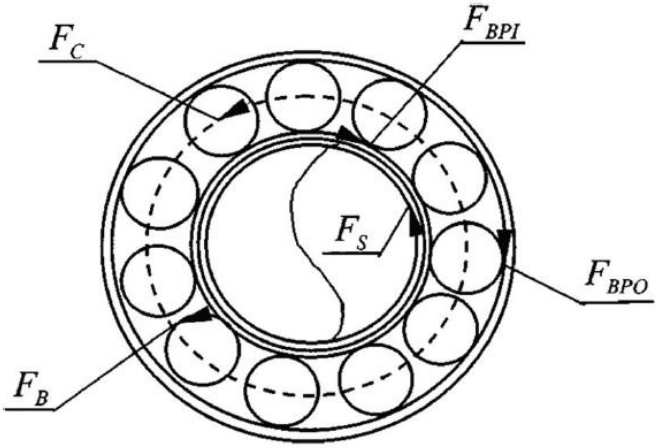

Fig 1.9: Frequencies of five basic motions of bearing.[5]

(a) Shaft Rotational Frequency (Fs): As bearings are often used to form a bearing–rotor system, the speed of the rotor (or shaft), Fs, is the most important movement of bearings. All other frequencies are a function of this frequency. Given by equation 1.

$$F_c = \frac{F_s}{2}\left(1 - \frac{B_d}{P_d}\cos\theta\right) \quad \text{(eq.1)}$$

(b) Fundamental Cage Frequency (Fc): The fundamental cage frequency, Fc, is the rotational speed of the cage (cage frequency). It can be derived from the linear velocity of a point on the cage, which is the mean of the linear velocities of the inner raceway and the outer raceway.

(c) Ball Pass Raceway Frequencies (F_{BPO} and F_{BPI}): These frequencies pertain to the rate at which the balls of the ball-bearing would pass over a groove in outer raceway (F_{BPO}) and a groove in inner raceway (F_{BPI}). Both these frequencies are the functions of the number of balls in a bearing, shaft rotational frequency and fundamental cage frequency.

$$F_{bpi} = \frac{Z}{2}F_s\left(1 - \frac{B_d}{P_d}\cos\theta\right) \quad \text{(eq.2)}$$

$$F_{bpo} = \frac{z}{2} F_s \left(1 + \frac{B_d}{Pd} \cos\theta\right) \ldots\ldots\ldots\ldots\ldots\ldots\ldots \text{(eq.3)}$$

(d) Ball Pass Frequency Rolling Element(F_B): This pertains to the rate at which a point (or a pit) on a rolling element (ball) of a ball-bearing would touch the inner and outer race ways. Ball Pass Frequency Rolling Element(F_B) is a function of the number of balls in a bearing, shaft rotational frequency, ball and pitch diameter.

$$F_b = \frac{z}{2} F_{\,s} \left(1 - \left(\frac{B_d}{P_d}\right)^2 \cos\theta\right) \ldots\ldots\ldots\ldots\ldots\ldots\ldots\ldots\ldots\ldots\ldots\ldots \text{(eq.4)}$$

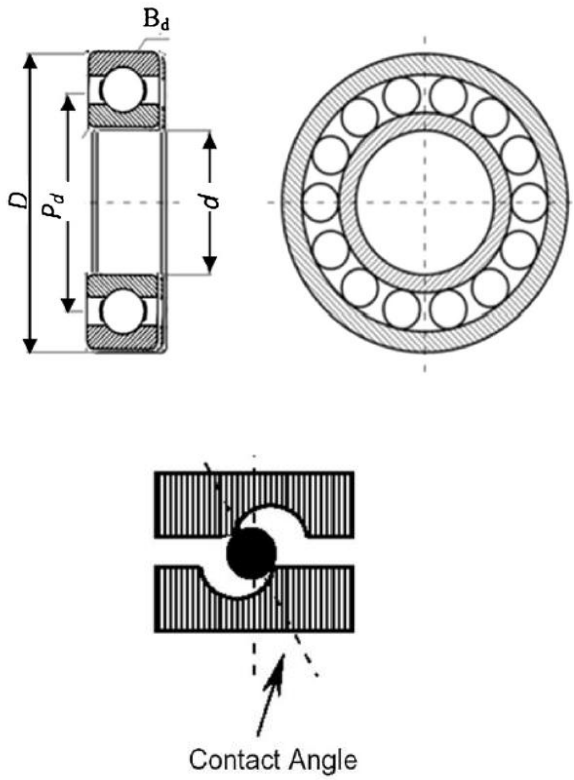

Fig 1.10: Basic dimensions [5]

where B_d is the ball diameter, P_d is the pitch diameter, Z is the number of balls, F is the shaft rotation frequency, D is outer diameter and d is inner diameter and θ is the contact angle.

1.7 Vibration Signal of Rolling Element Bearing Defects.

Bearing defect generates a series of impacts to which bearing response is a high frequency damped oscillation. These impacts occur periodically at bearing characteristic (defect) frequency, which is calculated from the geometry of bearing, shaft speed and type of defect. These defects generate a series of impacts as rolling element passes over the defect due to the metal to metal contact. The resultant vibration is characterised by sharp peaks in time domain signal. It is difficult to identify the defect frequency in spectrum as these impact vibrations distribute their energy over wide range of frequencies; the defect frequency of the bearing contains low energy and hence can be easily masked by noise and other low frequency effects. The frequency of occurrence of the impacts is the bearing characteristic defect frequency. These impacts excite the bearing structural resonant frequency.
response is a periodic burst of exponentially decaying high frequency oscillations (the bearing structural resonant frequency). The oscillations are of extremely short duration compared to interval between impulses, thus it is difficult to detect them in conventional frequency spectrum.

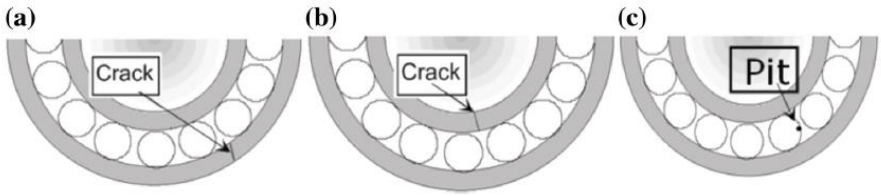

Fig1.11: Bearing defects an outer race fault. b Inner race fault. c Ball fault

1.8 Load Distribution

The loads carried by the ball and roller bearings are transmitted through the rolling elements from one ring to the other. As mentioned in [7], the relationship between load and deformation is:

$Q = k\delta^n$ ..... (eq.5)

where n = 1.5 for ball bearings and n = 1.11 for roller bearings, Q is the ball or roller normal load, d is the deformation, and k is the load-deflection factor. For a

rigidly supported bearing subjected to radial load, the radial deflection (δ_φ) at any rolling element angular position (φ) is given by:

$$\delta_\varphi = \delta_{max} \cos\varphi - \frac{1}{2} P_d \ldots\ldots\ldots\ldots\ldots\ldots \text{(eq. 6)}$$

in which δ_r is the ring radial shift, occurring at φ = 0 and P_d is the diametrical clearance.

Eq. 5 may be rearranged in terms of maximum deformation as follows:

$$\delta_\varphi = \delta_{max}\left(1 - \frac{1}{2\varepsilon}(1 - \cos\varphi)\right) \ldots\ldots\ldots\ldots\ldots\ldots \text{(eq. 7)}$$

Where ε is the load distribution factor given by:

$$\varepsilon = \frac{1}{2}\left(1 - \frac{P_d}{P_r}\right) \ldots\ldots\ldots\ldots\ldots\ldots\ldots\ldots\ldots\ldots \text{(eq. 8)}$$

Thus, for ball bearings under pure radial load and zero clearance, we get the well-known Stribeck's Eqn:

$$Q_{max} = \frac{4.37 F_r}{z\cos\varphi} \ldots\ldots\ldots\ldots\ldots\ldots\ldots\ldots\ldots\ldots\ldots\ldots \text{(eq.9)}$$

1.9 Diagnosis technique

To detect a defect in an early fault stage, different techniques and instruments have been developed depending on the range of frequencies within which the vibration analysis will be carried out. Some techniques have the high range frequency analysis approach; others have the medium and low range approach. The techniques which analyse the high frequency zone are based on the excitation of the natural frequency of the sensor, bearing parts and housing structures due to when such a defect on one surface strikes its mating surface, a pulse of short duration is produced (see Fig. 1.12). When the bearing rotates with a constant rotational speed, these pulses are generated periodically and the frequency is the characteristic defect frequency (Figure 1.12). High frequency waves produced due to a defect in the outer race. The main symptom that allows detecting incipient defects is the presence of components of high frequency. When the fault progresses, the impulsive excitation of type increases even up to a time until when the edges, corners or rims of the defects smooth down due to the wear and the impact levels diminishes and they can

even get to disappear. Most of the techniques of high frequency analysis give only an overall value of the energy caught by the sensor, which is compared with reference values and related to the severity of the defect. Within these techniques, there are the shock pulse measurement (SPM), the detection of acoustic emissions (AE), emitted spectral energy (SEE), technique of detection of high frequency (HFD) and the ultrasound. Other techniques of high frequency analysis related to the excitation of natural frequencies are the techniques of enveloping or demodulation and Peak Value or peak value analysis. Techniques that will be described briefly later in this work. In the high frequency analysis, there are two difficulties mainly, the first one is the low amplitude of the high frequency bursts compared with the components of low frequency. And second it is the difficult to identify the characteristic defect frequencies of the bearings due to the noise and the bad spectral resolution. To facilitate the tasks of diagnosis, it is necessary to isolate the high frequency vibrations from others using a high pass or band pass filters around the natural frequency that is excited. Thus, the vibration generated only by the impacts can be analysed identifying the discrete frequencies and evaluating the severity of fault.

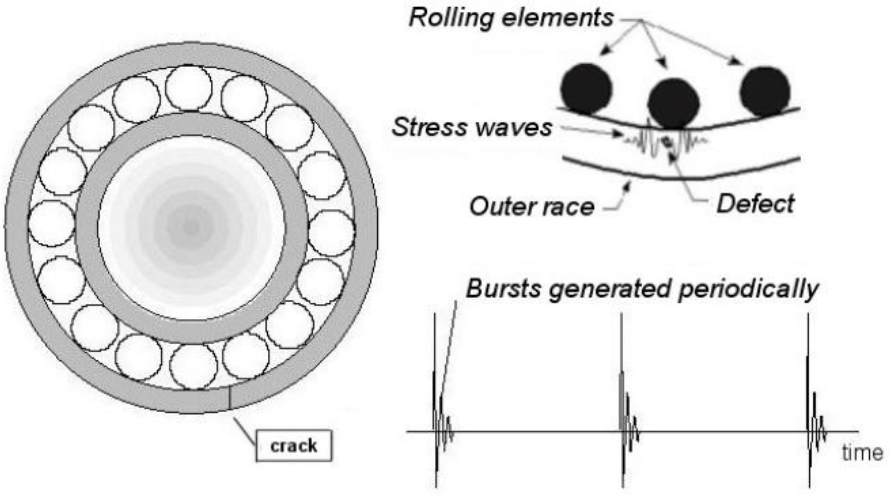

Fig 1.12: Impact pulse due to defect [7]

1.10 Impact force due to defect

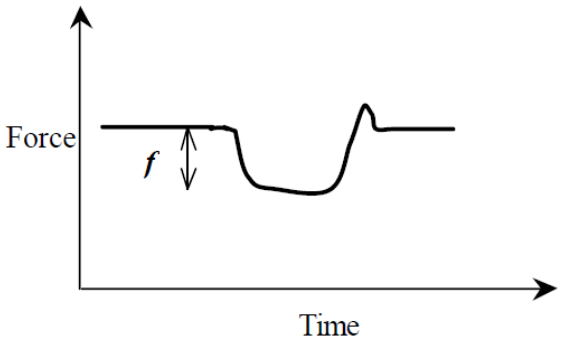

Fig. 1.3 Variation of force in the neighbourhood of a defect in the outer ring. [8]

Variation in the force exerted by the rolling element on the outer ring is seen when the rolling element passes over a defect. As the rolling element enters the defect, the force exerted tends to lessen in magnitude and the other rolling elements are forced to take up the load. This continues for as long as the rolling element is in the defect. When it impacts the other end of the defect, a surge in the force is seen because of the impact and then it decays to the value of the force exerted by the rolling element on the outer ring during normal operating conditions. Such a variation of forces would affect the vibration signal and would be captured by an accelerometer placed on the bearing. Typically, the decrease in the force by a value would be dependent on the depth of the defect and the time for which the value of the force would stay at that value would be dependent on the width of the defect.

1.11 Objective

The project is undertaken with objective to understand and analyse the localised fault in deep groove ball bearing with finite element model developed on Ansys work bench 15. With the help of finite model, investigation is carried out to develop a comprehensive plethora, where in different size and shape of localised faults can be studied. The intent is to summarise the effect of varying defect size on impact and vibration created in bearing and thus giving insight to understand future problems created by them. A trend is attempted to be established to compare the different faults for further research. The project also aims to garner the feasibility and understanding the FEA in fault diagnostic and analysis.

1.12 Organisation of thesis

A brief overview of the contents discussed and presented in the project report

Chapter 1: This chapter contains overall theoretical description of the concept of bearing faults their causes and bearing definitions. The effect off localised fault on impact forces leading vibrational noises have been explained with the diagnostic approach.

Chapter 2: Chapter contains brief summary of different research work in the area of bearing faults and finite element modelling which have been the basis of the project work. A crisp discussion of previous research has been made.

Chapter 3: This chapters deals with design and simulation stage. Here geometry and material properties have been given. The simulation stages along with the boundary condition, contacts, solvers and analysis settings are explained

Chapter 4: This chapter contains results and discussion, where individual simulation results have been discussed long with a deep comparative analysis is done to deduce trends and conclusions.

Chapter 5: Conclusions of the project work have been given in most concise and objective manner.

CHAPTER 2: LITERATURE REVIEW

Ball bearing fault modelling, simulation and condition monitoring using vibrational, acoustic, thermal parameters have been areas of constant research for very long and are ever evolving with implementation of computational techniques. Various researches have been studied in order to reach my goals of modelling and analysing localised faults in deep groove ball bearing and thus it is incumbent on me to discuss them in brief.

Cotogno M. and Pedraza E. [1] developed an elasto-dynamic model of a defective sphere bearing is presented. This two-dimensional model can simulate local faults on the bearing races and rolling elements, and it is based on the non-linear Hertzian contact deformation of the rolling elements. In the model, the outer race is supposed to be fixed, and the rolling elements are supposed to roll without slipping. These assumptions yield a total of $z + 4$ Degrees of Freedom (DOF), where z is the number of rolling elements: three DOF come from the inner race (two displacements and one rotation), one DOF from the cage (rotation) and one DOF from each rolling element (i.e., z radial displacements). Each contact between the spheres and the races is modelled by a non-linear spring (Hertz contact theory) and a damper proportional to the spring stiffness (Palmgren). The model uses a kinematic approach to calculate the trajectory of the rolling elements when passing over the defect. This trajectory is introduced into the equations of motion for the calculation of the rolling elements deformations; subsequently, the internal bearing forces are calculated. The model inputs are the bearing and defect geometry, the materials characteristics and the radial load. The model outputs the overall force transmitted to the outer race, which accurately reproduces the typical behaviour exhibited by a faulty bearing both in time and frequency domain.

Shaky, Darpe and Kulkarni [2] , did a comparative analysis of different of different tools to interpret the vibration signals of a faulty bearing and identify the behaviour of the defects. From the analysis, it is evident that among the various time domain, frequency domain and time-frequency domain parameters studied, the HFRT DFA of the time domain vibration data and the HFRT DFA of the CWT time slice data are best suited for early damage identification for all the cases considered. On the

overall ranking of the parameters, the HFRT DFA obtained from the raw time domain data and from the time slice of the CWT data (at the resonance frequency) are among the best parameters, while the FFT-based parameters, such as the amplitudes of the DF and its harmonics, are relatively poor for any kind of defects.

Nabhan and Nouby examined [4] the contact stress distribution of deep groove ball bearings through analytical and numerical methods. The contact pressure distribution between the ball and the raceway of the bearing 6004 is performed by finite element software ABAQUS. To validate the finite element model, an analytical method using Hertzian contact theory was derived by MATLAB software. Influence of shaft misalignment with different angles was investigated. It was found that finite element analysis can be evaluated the contact stress at any point around the contact surface. It was also concluded that the shaft misalignment lead to decrease the maximum contact stress and increase the contact area between the ball and the raceway of the bearing.

Emil Claesson [5] worked on three simplified FE-models for roller bearings, both cylindrical and tapered bearings, had been developed. The models had different levels of complexity and computational cost. The cylindrical models had been verified against reference results from full FE-models with satisfactory result. The models for tapered bearings are still to be verified.

Fleming and Poplawski [6] analysed rolling-element bearing forces that vary nonlinearly with bearing deflection. Thus an accurate rotor dynamic for non-linear transient analysis required bearing forces to be determined at each step of the transient solution. Analyses had been carried out to show the effect of accurate bearing transient forces (accounting speed and load- dependent bearing stiffness) as compared to conventional use of average rolling element bearing stiffness. Bearing forces were calculated by COBRA-AHS (Computer Optimized Ball and Roller Bearing Analysis—Advanced High Speed) and supplied to the rotor dynamics code ARDS (Analysis of Rotor Dynamic Systems) for accurate simulation of rotor transient behaviour. COBRA-AHS is a fast-running five degree-of-freedom computer code able to calculate high speed rolling-element bearing load-displacement data for radial and angular contact ball bearings and also for

cylindrical and tapered roller bearings. Results show that use of nonlinear bearing characteristics is essential for accurate prediction of rotor dynamic behaviour.

Kulkarni [7] proposed simulation method is used to determine the vibration signal response for various shaft speeds and loading condition, which is compared with experimental result. It was found simulated vibration pattern had similar characteristic compare to experimental results. The deviation in amplitude of acceleration is may be due to variation of mesh density in the region near to defect and also deviation in frequency occurs due to uncontrolled parameters during experimentation. It was observed that as the speed increases the peak amplitude values (m/s2) gradually increased for constant load. Also the peak amplitude values (m/s2) for healthy bearing are smaller than defective bearing. It was found that the amplitude values for the case of outer race defect were more than that for the inner race defect. It was because of defect present on the outer race was remained in the load zone at maximum position as in second case, inner race moved in and out of the load zone during each revolution of the shaft. The strong fault vibration spectrum produced while the defect was in the load zone and weaker fault vibration spectrum produced while the defect was outside the load zone.

Mathew J. and Alferdson R. [8] developed the technique of condition monitoring for rolling element bearings by using vibration analysis. The vibration data were analysed and several parameters [Peak Level, RMS Level, Matched Filter RMS, Kurtosis Factor] were assessed with regard to their effectiveness in the detection of bearing condition it was found that all the parameters were having some value depending on the type of bearing failure encountered. Frequency domain parameters were more consistent in the detection of damage than time domain parameters. They have suggested it would be unreliable to depend exclusively on any one technique to detect bearing damage.

McFadden defect and Smith [9] presented a model for the vibration created by a single point in a rolling element bearing. It indicates the vibration produced by a single point defect on the inner race of a rolling element bearing under constant radial load. The model integrates the shaft speed, effects of bearing geometry, bearing load distribution, transfer function and the exponential decay of vibration. The vibration is modelled as a product of a series of impulses at rolling element

passing frequency with bearing the load distribution and the amplitude of a transfer function, convolved with the impulse response exponential decay function. The model is used only to a single point defect on bearing inner race under radial load. Extension of the model to include multiple point defects and outer race and rolling element defects under radial and axial load is required.

McFadden and Smith [10] showed that the vibration created by multiple point defects in a rolling element bearing. A model for the high frequency vibration formed by a single point defect on bearing inner race under radial load is extended to describe the vibration produced by multiple point defects. The phase angles were derived for defects at any position on the inner race and superposition was used to give the vibration spectrum. The performance of the model will be confirmed by experiments on a bearing with more defects on its inner race.

Sunnersjo C. [11] has given clarification about the relationship between geometrical imperfections of the bearing components and resulting pedestal vibrations during operation. A mixed theoretical and experimental impedance approach has been used to treat the bearing when fitted into a simple machine structure. Further, it shows how resulting vibrations of the bearing pedestal can be calculated. It highlights possible methods of condition monitoring and prediction of impending bearing failure. This method is useful for lightly loaded bearings operating at low and moderate speeds.

Y.hland E [12] presented a linear theoretical model for the vibrations of a shaft bearing system produced by ball bearing geometrical imperfections. It is usable for low and medium speeds where ball centrifugal forces can be omitted. The excitation forces from each bearing are considered and can serve as input to suitable rotor dynamic programs. Imperfections shielded are radial and axial waviness of outer and inner rings, non-uniform cage pocket distribution, ball waviness and diameter distribution. Explicit rules are demonstrated in the bearing stiffness matrix, the influence matrix of form errors and the form error vector, the three central concepts of the mannequin. The answer to the non-linear equilibrium equations of the same shaft-bearing arrangement is expected to be recognized if the bearings are geometrically perfect. The example of rotating outer ring and stationary inner ring requires minor modifications. Minor variations in groove radii are readily brought

out as an additional case of configuration error. The enlargement of the model to cover the centrifugal action of the balls. The incorporation of roller bearings into the mannequin is very much a question of how accurately the (non-Hertzian) contacts encountered have to be treated. Lightly loaded roller bearings with optimized roller profiles have non-Hertzian contacts, already at low load, and cause considerable complications. The extension of the model to work in a more general environment, like coupling to flexible pedestals. Modern computational methods developed in structural dynamics should be immediately applicable.

Tandon N. and Choudhury A. [13] presented an analytical model for the vibration response of rolling element bearings due to a localized defect. The amplitudes of significant frequency components on inner race\ outer race or on one of the rolling elements under axial and radial loads. The model forecasts a discrete spectrum having peaks at the characteristic defect frequencies and their harmonics. And it predicts the effect of load and pulse shape on the vibration amplitude has been considered in the model. The example presented here predicts a frequency spectrum having peaks at characteristic defect frequencies with modulations in the shell of a rolling element defect and an inner race defect under a radial load. The amplitudes at these frequencies are also called for various defect locations. The amplitude of the outer race defect is found to be quite high in comparison to those for the inner race defect and the rolling element defect. The amplitude level is likewise set up to increase with an increase in load and it is represented by the configurations of the generated pulses. The analytical and experimental values agreement is limited to the elements at the inner race defect frequency and sidebands about this component at multiples of the beam frequency.

Choudhury A. and Tandon N. [14] have been presented an analytical model to forecast the vibration response of rolling bearings due to distributed defects under radial load. For bearings without defect and with race defect, the model prophesies a discrete spectrum with components at outer and inner race characteristic defect frequencies for the response of the respective races. The amplitudes for race defects increase considerably in comparison to the amplitudes at corresponding frequencies for a bearing without defect. For a bearing with off-size rolling element, the response of the outer race is at cage frequency and its multiples. The response of inner race is created to be at the relative frequency of inner race with respect to cage

along with sidebands at shaft frequency and its multiples. The results can be compared with FEM and experimentation. The model can be extended for radial and axial load.

Fawzi M.et al [15] studied the effect of the outer ring ovality on the dynamic behaviour of rotating machinery under rotating unbalance with consideration of ball bearing nonlinearities, shaft elasticity, and speed of rotation. The equations of movement of a rotor–ball bearing system are formulated using finite-elements FE discretization and Lagrange's equations. The analyses are specified to a rigid-rotor system, by retaining the rigid body modes only in the FE solution. The time domain and frequency domain techniques were used in a system with and without outer ring ovality. It is found that with ideal bearings, no ovality, the vibration spectrum is qualitatively and quantitatively the same in both the horizontal and vertical directions. When the ring ovality is introduced, however, the spectrum in both orthogonal planes is no longer similar. And the magnitude of the bearing load has improved in the form of repeated random impacts, between balls and rings, in the horizontal direction of maximum clearance compared to a continuous contact along the vertical direction of positive zero clearance. This underlines the importance of the vibration measuring probe's direction, with respect to the outer ring axes, to capture impact-induced vibrations. When the harmonic excitation is increased in a system with ideal bearings, the spectral peaks above forcing frequency have shifted to a higher-frequency region, indicating some sort of a hard spring mechanism inherent in the system. Another observation is that for the same external excitation, vibration amplitude at forcing frequency in the bearing force spectrum is the same for systems with or without outer ring ovality. The adopted modelling approach, that is solved for a rigid shaft system using existing FE codes for rotor dynamics, can be used for inner ring also. It has to be validated by experimentation for outer and inner rings.

Aktuerk N. and Gohar R.[16] shown the effect of ball size variation on vibrations associated with ball-bearings. The axial and radial vibrations of a rigid shaft obtained by a pair of angular contact ball-bearings are studied. The theoretical model model and a computer program were developed to simulate this effect and the results presented in frequency and time domains. All results show that off-sized balls in the bearing cause vibrations at cage speed and its harmonics, depending on

their arrangement within the bearing. Symmetric combinations will produce vibrations at the multiples of the cage speed and all other combinations will produce vibrations at the cage speed. If only one ball is oversized when the diameter difference increases, the peak-to-peak amplitude of the vibrations will also increase. The effect due to more than one ball oversized is yet to study.

Brian T. Holm and Hansen Robert X. Ga [17] studied the vibrational behaviour of a deep groove ball bearing with a structurally integrated force sensor. The miniaturized force sensor fitted within a slot on the bearing, provides real time condition monitoring of the bearing. Mathematical and FE models were developed to predict the sensor output due to bearing dynamic load and rotational speed variations. Experimentation was conducted on a ball bearing to validate the mathematical and FEA solutions. The results confirm the approach of integrated-sensing for bearing condition monitoring. Future research will emphasis on creating efficient and advanced signal processing techniques using neural-fuzzy networks and wavelet transform to relate signal features to specific bearing faults. Also, further experimental studies will be conducted on a better-quality bearing test bed that permits for a much wider range of operating conditions to be examined. The joint theoretical and experimental work will make a strong basis for the development of an integrated real time bearing condition monitoring. The model will provide early defect warning to a wide range of ball bearings and manufacturing equipment.

Prabhakar, Mohanty and Sekhar [18] investigated faults in ball bearing by application of DWT. Vibration signals from rolling contact bearings having single and multiple point defects on outer race, inner race and the combination faults have been observed for analysis. In wavelet decompositions, the impulses in vibration signals due to bearing faults are prominent. It is observed that according to characteristic defect frequencies impulses come out periodically with a time period. For detecting single and multiple faults in the ball bearings DWT can be used as an efficient instrument.

McInerny and Day [19] presented a laboratory module for fault detection in rolling element bearings. The formulas given for the deliberation of the characteristic fault frequencies and backdrop on the basic operational features of ball bearings is

presented. The defects of conventional vibration spectral analysis for the detection of bearing faults is observed in the setting of a synthetic vibration signal that students generate in MATLAB. The vibration signatures measured on bearing housings shares several key features Envelope analysis and the connection between bearing fault signatures and amplitude modulation /demodulation are explained. Lastly, a graphically driven software utility is inserted. This software helps to explore envelope analysis using measured data or the synthetic signal that they created. The software service program and the material introduced in this paper establish an instructional module on bearing fault detection. After surveying the basic performance of rolling element bearings and the characteristics of idealized bearing fault vibration signatures, the defects of conventional spectral analysis were illustrated with a synthetic signal generated in MATLAB.

M Amarnath et-al [20] established the technique to give early information about progressing malfunctions. To monitor the condition of antifriction bearings and to understand the details of severity of defects before they cause serious catastrophic failures. The vibration monitoring technique is worthy to analyze various defects in bearing. Frequency domain analysis, time domain analysis and spike energy analysis have been used to identify different defects in bearings. The outcomes have validated that each one of these techniques is useful to investigate problems in bearings. Frequency spectrum identifies the exact nature of defects in bearings and time waveform indicates severity of vibrations for defective bearings. The spike energy level, which is more comprehensive parameter to predict the severity of the defect in antifriction bearings in the bearings, was also recorded for all bearings.

Xinsheng Lou et-al [21] presented a technique to diagnosis bearing fault based on wavelet transform and fuzzy inference. The analysis of defects in ball bearings based on the wavelet transforms and Neuro-fuzzy classification. Vibration signals for healthy bearings, bearings with ball faults and race faults were captured from an experimental system. The wavelet transform was used to generate feature vectors by processing the accelerometer signals. An adaptive neural-fuzzy inference system (ANFIS) was used as a diagnostic classifier. For comparability purposes, the Euclidean vector distance method as well as the vector correlation coefficient method was also looked into. The developed diagnostic method can reliably separate different fault conditions under the presence of various loads.

V. Purushothama and S. Narayanana [22] demonstrated a suitable condition monitoring process to prevent malfunctions and breakages during operation. The method for detecting localized bearing defects based on wavelet transform. Bearing race faults found by using discrete wavelet transform. Vibration signals from ball bearings having a single and multiple point defects on outer race, inner race, ball fault and combination of these faults considered for analysis. Wavelet transforms gives a variable resolution time–frequency distribution. It is shown that the impulses created periodically with a time period corresponding to characteristic defect frequencies. The diagnoses of ball bearing race faults have been found using wavelet transform. These results are compared with feature extraction, data and results from spectrum analysis. It also presents a novel method of pattern recognition for bearing condition monitoring using hidden Markov Models. Experimental results shows that successful bearing fault detection rates as high as 99% can be achieved with this plan of attack. It has been shown that DWT can be used as an efficient instrument for detecting single and multiple faults in rolling contact bearings.

R. K. Purohit and K. Purohit [23] studied the axial and radial vibrations of a rigid shaft supported bearings are considered. The effect of vibrations of varying the number of balls and preload in the bearings is studied for prefect bearings. In the mathematical formulation, the contacts between the races and the balls are considered as nonlinear springs. The stiffness is obtained by using the Hertzian elastic contact deformation theory. The numerical integration technique Newmark-b with Newton-Raphson method is used to crack the nonlinear differential equations iteratively. For healthy bearings, vibrations occur at the ball passage frequency. The amplitudes of these oscillations are noted to be considerably scaled down if the preload and number of balls are correctly chosen. All results are obtained in the form of Fast Fourier Transformations.

A Choudhury And N Tandon [24] showed the vibration response of ball bearings in a rotor bearing system to a local defect under radial load. In the present research, a theoretical model has been established to generate the vibration response due to a localized defect in various bearing components in a rotor-bearing system under radial load conditions. The experimental setup on which the theoretical results have been validated has been modeled as a multi-DOF system. In this study poor

agreement for the harmonics of shaft and cage frequencies in the case of an inner race defect and rolling element defect respectively. This was expected because the components at harmonics of shaft frequency primarily occur due to rotor malfunction such as residual unbalance, misalignment etc. which have not been considered in the theoretical model.

Mohamadi Monavar, Ahmadi and Mohtasebi [26] investigated a technique to forecaste defects in bal bearings using vibration signal analysis. The vibration monitoring technique is suitable to analyze various defects in bearing. This technique gives early information about progressing defects. Triaxial vibration measurement technique was used at each terminal of the pairing of the motor and rotor bearing housings. Time waveform specifies severity of vibrations for defective bearings and vibration spectrum indicates the precise nature of defects in bearings. The answers propose that bad bearing has a substantial force on the vibration spectra. Time domain analysis, vibration spectrum analysis has been utlised to identify different defects in bearings. The outcomes have verified that each one of these techniques is useful to find problems in bearings.

Arun Kr. Jalan and A. R. Mohanty [27] presented technique for error diagnosis of rotor-bearing system was considered. The residual generation technique was employed for detection of errors due to misalignment and imbalance. The residual powers are compared with the equivalent theoretical forces. The fault condition and position of flaws are successfully discovered by this proficiency. This method may be useful for large systems like turbine shafts and gear boxes.

Feng Wang, Yu Bo Li, and Zhi Gao Luo [28] presented a novel method to realize classification of fault signal without extracting feature vector. By calculating the time delay and embedding dimension of time series, vibration, signal is reconstructed into phase space and Gaussian mixture model was made for every sort of fault signal in the reconstructed phase space. It was shown that this method is effective for classifying not only fault types but also fault severity. Information obtained by examining the time series only so it is very suitable for industrial application.

Patil and Kumar [29] investigated experimentally the influence of the defect size on ball bearing vibration using Wavelet Transform. An analytical model is presented

for predicting the effect of a localized defect on the ball bearing vibrations. In the mathematical modelling, the contacts between the races and the ball are incorporated as non-linear springs. The contact force is found using the Hertzian contact deformation theory. A computer program is developed to simulate the defect on the raceways with the solutions given in the frequency domain and time domain. The model produces both the frequency and the acceleration of vibration components of the bearing. The consequence of the defect size and its placement has been studied. This investigation is cantered towards the growth of a mathematical model to find the issue of defect size on bearing vibration. Instead of using periodically repeated impulse function for the impulse due to defect, defect itself is modeled as part of sinusoidal waves. The present model is fairly limited in treating the ball skidding effect. The present effort was targeted at a more elementary approach to obtain a theoretical model to analyze the issue of defect size, load and speed of the bearing vibration and predict the spectral components. Including the ball raceway interaction and the ball skidding phenomenon would make the model more rigorous. Nevertheless, this model will be promoted at a future time to contain the issue of ball skidding to predict the spectral components of giving birth with defects.

Cong J et-al [30] investigated bearing faults are among the main causes of breakdown in rotating machines. In this study, a bearing fault model is suggested based on the dynamic load analysis of a rotor-bearing organization. The rotor impact factor is taken into consideration in the rolling bearing fault signal model. The defect load on the airfoil of the bearing is divided into two sections: the determinate load and the alternate load. The vibration response of the proposed fault signal model is investigated and the fault signal calculating equation is derived through dynamic and kinematic analysis. Outer race and inner race fault simulations are seen in the composition. The simulation process includes consideration of various parameters, such as the gravitational force of the rotor-bearing system, the asymmetry of the rotor, and the position of the shortcoming on the airfoil. The simulation result shows that different amplitude combines the alternate load and determinate load will cause different envelope spectrum expressions. The rotating frequency sidebands will arise in the envelope spectrum in addition to the fault characteristic frequency. This appearance of sidebands will produce the difficulty

of fault recognition in intelligent fault diagnosis. The proposed results of signal model simulation have successfully validated by experimentation

Chunjun [31] presented paper on Static Analysis of Rolling Bearings Using Finite Element Method. In this he did Static Analysis of Angular Contact Ball Bearing, Contact Analysis and Simulation of Angular Contact Ball Bearing with Simplified Model Using Beam Element. He fined the reasonable reference reaction force from the outer ring to the inner ring by means of FEM simulation. Also, instead of using ball, to simplify the rolling bearing with some other elements between the inner and outer ring. The model mainly used to be discussed is angular contact ball bearing. To do the simulation with the part model of bearing, flexible model has to be used for the rings and ball. The model with beams between the inner ring and outer ring will be used to simplify the angular contact ball bearing.

lin [32] analysed the displacement and the coefficient of Stiffness for radial ball bearings with angular contact from the production of SKF. For the analysis John Harris's method based on the theory of Hertz-contact has been used. In order to compare the results obtained by the mentioned method and Palmgre n's empirical relations the finite element method has been used.

Matej Tadina [33] developed comprehensive model of a ball bearing was developed to obtain the vibration response due to localised defects. For the purpose of simplification, the inner ring of the bearing had only 2 DOF and the centrifugal load effects were included. The proposed model includes several new considerations. The outer ring was deformable and is modelled with finite elements, and can be coupled with an arbitrary housing structure if it was discretized with finite elements. The contact force between the outer race and the ball was moving16 within the finite element continuously, and due to this the finite element can be larger and the final model was computationally less demanding. The contact properties were described with detailed geometrical properties and small changes in the contact stiffness are taken into account. The developed bearing model was used to simulate the vibration response of the bearing/pedestal system due to different local faults, while the shaft’s rotational frequency was increasing. Although the rotational frequency was non-stationary, the envelope analysis method could identify all the local bearing defects. The time interval for the envelope analysis had to be taken carefully, since

the defect on the bearing element has to be in the loading zone in that time interval, but the time interval had to be short enough so that there was only a small change in the shaft's rotating frequency. The signal used for the envelope analysis had to be zero padded to had a sufficient frequency resolution, where we had to be aware of the limitations and consequences of zero padding. On other hand, the CWT gave the same results, where the analysed time interval can be taken as arbitrary to identify the bearing faults.

Azzam [34] addresses Rolling Contact Fatigue (RCF) occurred due to the result of cyclic stress developed during operation and mechanism that involved in fretting failure of rolling element bearing. As bearing raceways of non-rotating rolling element bearings exposed to vibration or sliding oscillation false Brinelling occurs. Bearing surface due to false Brinelling tends to damage within a short period, due to cavities created on the bearing raceway. Recommendation towards enhancement of bearing life was also suggested.

Weimin Ding and Zhinan Zhang [35] proposed a numerical approach on identifying the vibration response of a ball bearing with three different sizes of defects on the outer raceway. A 3-D finite element rigid bearing model with the aforementioned defects were built and numerically solved with the ABAQUS dynamic explicit solver. The vibration response of the model was monitored through recording the displacement of the monitor node, which is centrally located at the top of the bearing house's outer surface. By analysing the simulated vibration signals, the characteristic frequencies of different defects were distinguished. Several high-order defect frequencies can also be distinguished. The validation of the numerical approach was proved. The numerical simulation also examines the effects of the defect sizes. Three different sizes of defects were numerically simulated in the finite element model. It is showed that the stiffness of the bearing model decreases when the rolling ball drops into a defect, thus an impact wave is excited. The impact effect of the defect is in positive correlation with the defect size. The larger the defect, the stronger the amplitude of characteristic frequency of the defect will be. The waveform is closely related to defect size. The time separation between the moment when rolling balls enter and exit the defect can be used to estimate the defect size (circumferential length).

Wei Guo, Hongrui Cao, Zhengjia He, and Laihao Yang [37] proposed quasistatic model considering mechanical properties of whole bearing was introduced into the fatigue life calculation of angular contact ball bearing. Then, a coupling model of fatigue life and damage was established for rolling bearing. The fatigue life of bearing parts was analysed under different rotational speed, axial load, and radial load. The results have shown that different working condition has a great influence on fatigue lives of bearing parts, under setting conditions in this paper, specifically as follows: (1) With the increasing of rotational speed, the fatigue life of inner raceway and rollers is up while of outer raceway decline. The rotational speed does not much affect the order in which the damage appear on bearing parts. (2) The fatigue life of three parts decreases with the axial load increasing, the fastest of which is the life of inner raceway. The rolling elements and raceways are damaged in different order under different load value. The inner raceway is easiest to emerge failure when axial load is higher than 29 kN. (3) As radial load increasing, the fatigue life of outer raceway and rollers falls while of inner raceway rising a bit. The rollers are easiest to damage when load is larger than 5 kN.

Jing Liu and Ming J Zuo. [38] examined the effects of the defect shape, radial load and shaft speed on the pulse waveform characteristics generated by localized defects using the method of explicit dynamic finite element analysis. To validate the proposed model, the results obtained from the experiments had also been provided, and the waveform and the duration of the pulse generated by the defect on the outer race were in good agreement with the simulation results, which shows validation of the proposed model. Both the experimental results and the simulation results have confirmed that the impulse shape generated by the defect on the raceway will be influenced by the contact deformations at the edges of the defect. The results obtained also demonstrate that the explicit dynamic finite element analysis approach can be used to analyze the pulse waveform characteristic generated by localized defects in ball bearings.

Zhinan Zhang, Weimin Ding, and Huifang Mai [39] developed a finite element model of deep groove ball bearing with an artificial round defect on outer raceway. The simulation was performed based on explicit dynamic finite element software, ABAQUS. The process of rolling balls passing through defect zone was divided into five stages. The effects of radial load, rotation speed, and initial defect size on

the stress level were analyzed. This work complements the research about stress concentration phenomenon in rolling bearings. The conclusions drawn from the study can be summarized as:1. Higher Mises stress and contact pressure were generated during the rolling balls passing through the defect.2. The maximum Mises stress and contact pressure increased with the increase in radial load. The simulated maximum contact pressure of defect free zone agreed with the calculated results very well.

The literature review shows that primary focuses of researchers in past has been on condition based monitoring techniques (CBM) for analyzing bearing faults. Most of the emphasis is laid on the signal processing techniques of the vibrations captured from the setup containing faulted bearings. Time domain and frequency domain studies have been done very often for CBM. Since it is difficult to identify incipient bearing defects in the frequency spectrum, many specialised techniques have been developed over the years for bearing fault diagnosis, such as, Bi-spectrum coherence, spectral entropy, autoregressive models, envelope spectrum wavelet transform and more Artificial Neural Network (ANN) to machinery fault diagnosis. There has been very less efforts made in using finite element analysis to model and simulate the faults in bearings. Finite element models can be developed to study the behavior and detrimental effects of the bearing faults and to predict the unforeseen failures associated with the defects developed in the ball bearing over the time.

CHAPTER 3: METHODOLOGY

In this chapter, there is detailed discussion and explanation of design of deep groove ball bearing selected for the simulation and modelling process. There is brief description of the methodology for the process followed during the simulation process. The basic structure for this section includes

- Design description of the bearing that includes dimensions and material properties along with the defect description
- Steps followed on Ansys workbench 15 during simulation.
- Defining contact properties and coordinate system.
- Explanation of meshing process.
- Defining boundary conditions and loads.
- Solver and analysis controls used.

3.1 Design

The 6200-deep groove ball bearing is used to analyse the localised fault in inner race and description of bearing geometry, material and localised fault sizes has been detailed out subsequently

3.1.1 Bearing parameters

Table 3.1: Bearing geometry

Bearing part name	In mm	Parameter name	In mm	Parameter name	In mm	Parameter Name	In mm	Parameter name	Value
Bearing outside diameter	30	Bearing bore diameter	10	Bearing width	9	Ball diameter	6	Number of balls	8
Rib diameter of outer ring	23.8	Bearing bore diameter	17.4	Raceway diameter of outer ring	25.27	Raceway diameter of inner ring	15.738	Radial load	5000N
Raceway groove curvature radius of outer ring	2.49	Raceway groove curvature radius of inner ring	2.44	Pitch diameter of ball set	20.5				

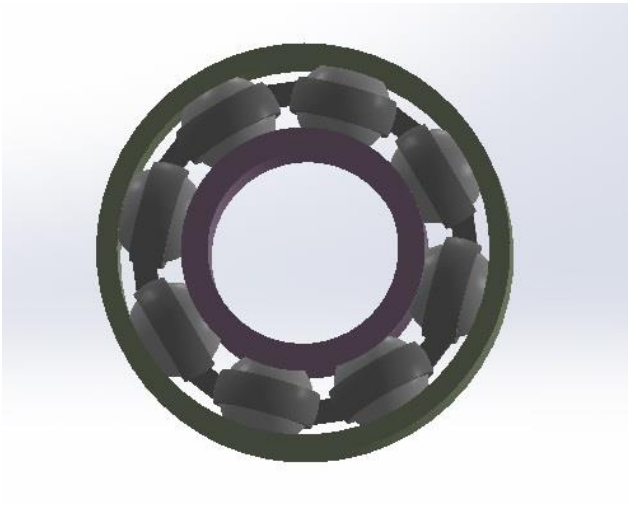

Fig 3.1: Assembly view of ball bearing on solid works.

3.1.2 Material properties

Table 3.2. Material properties

Bearing part name	Material	Modulus of elasticity(N/mm)	Density(kg/m3)	Poisson's ratio
Inner ring	GCr15SiMn	2.16×10^{11}	7820	.3
Outer ring	GCr15SiMn	2.16×10^{11}	7820	.3
Rolling element	GCr15SiMn	2.16×10^{11}	7820	.3
Cage	Yellow brass	1.0×10^{11}	8500	.324

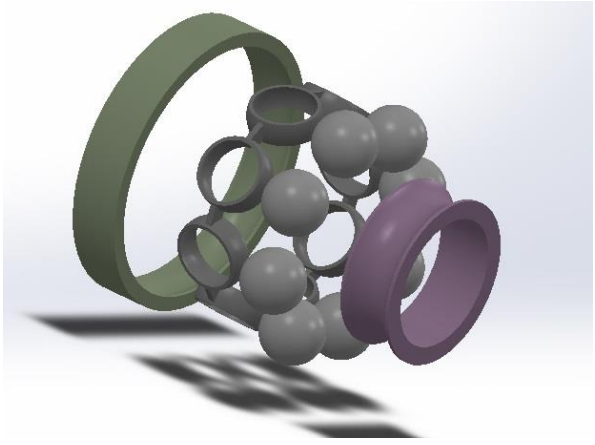

Fig 3.2: exploded view of deep groove ball bearing

2 types of defects have been introduced in the inner race of ball bearing which have been modelled as cylindrical point defect and rectangular point defect to emulate the effect of localised defect on the ball bearing.

Table 3.3: list of defects and their dimensions

Type 1: Cylindrical Defect (in mm)	Type 2: Square defect (in mm)
.05 diameter and .1 depth	.05x.05 (LXb) and .1 depth
.1 diameter and .1 depth	.1x.1 (LXb) and .1 depth
.2 diameter and .1 depth	.2x.2 (LXb) and .1 depth
.3 diameter and .1 depth	.3x.3LXb) and .1 depth
.4 diameter and .1 depth	.4x.4 (LXb) and .1 depth

Fig 3.3: Defect type 1

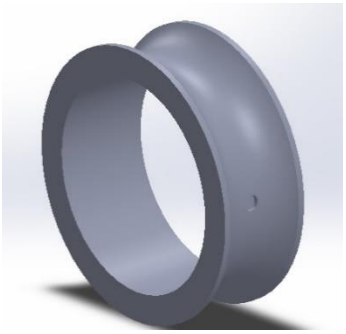

Fig 3.4: Defect type 2

3.1.3 Design process and software

Solid Works 14 has been used to develop the models of deep groove ball bearing where individual parts were made as part files using 2-d drawing and then making them into 3-d features for the individual parts. Once the cage, outer race, inner race and ball have been individually modelled then using assembly features the mates were created and whole ball bearing model was developed. For modelling the defect, the individual part files of the races were changed and induced with the defect thus thereby implicating those modification directly into the assembly of the ball deep groove ball bearing. IGS format was used to incorporate the files for their smooth retrieval in the Ansys work bench 15.

3.2 Defining contacts and Connections.

Once the geometry has been imported to Ansys workbench then the main work is on design modeler where the first basic steps is form the local cartesian coordinate system for the ball bearing and cylindrical coordinate system is also defined for the inner race for introducing the revolute joint at inner race. Then there are 24 contacts in the model where there are the main types of connections are 5.

The basic steps in the bearing contact settings**.**
In contact problem involved two boundaries, it is natural that take one boundary as target surface and take the other one as contact surface. Surface-surface contact is very suitable for those problems just as: interference fitting installation, or embedded contact, forging and deep-drawing. Typical surface-surface contact's analysis steps mainly include:
Build 3D geometry model and mesh.

- Identify contact pairs
- Name target surface and contact surface
- Define target surface
- Define contact surface
- Set up element key options and real constants
- Define and control rigid Goal's movement (only applicable in rigid-flexible contact)
- Apply the necessary boundary condition.

ANSYS supports surface contact elements of rigid-flexible or flexible-flexible. The elements form contact pairs by using target and contact surface. For the rigid-flexible contact, it can be chosen as contact surface such as convex surface, dense meshing or little size surface, otherwise chosen as target surface.

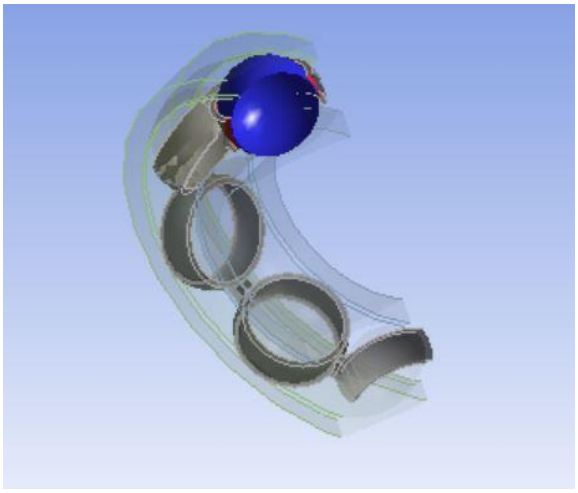

Fig 3.5: Contact between cage to ball

3.2.1 Cage to balls contact

The contact between ball and their retainers are taken as frictionless and there are such type of 8 contacts in the model.

When choosing a formulation to be used in a contact region, you basically decide the mathematical method that the code will use to enforce the contact compatibility condition (for example, no penetration allowed, no separation, no sliding, or sliding with some resistance).

3.2.2 Contact formulation

There are four basic contact formulations available in Ansys 15 and these are enlisted below.

- Penalty method
- Augmented Lagrange
- Pure Lagrange
- Multipoint constraint (or MPC)

The penalty method introduces a force at the contact detection point(s) that has penetrated across the target surface with the express purpose of eliminating the penetration. This method uses very simple formulas:

$F_c = k_c * D_p$ ……. (eq.10)

for contact detection points that penetrate across the target, and

F_c = zero……. (eq.11)

for open contact detection points. k_c is the contact stiffness (also called penalty stiffness); it is a predetermined property of the contact element. D_p is the penetration at the contact element. Hence, the larger the penetration, the greater the calculated force. The challenge here is that the magnitude of the force necessary to prevent penetration is completely unknown beforehand. Obviously, the force needs to be large enough to push the contact surface back to the target surface and, thereby, eliminate unwanted penetration but not so large that it pushes the contact completely off the target surface, causing error and instability. A positive aspect of the penalty method is that it is elegantly simple. The negative is that you end up with a finite amount of penetration at the end of the load step. Of course, this penetration is necessary for a contact force to be generated. It is important, therefore, that the contact stiffness be large enough so that the resulting penetration is negligibly small; but the contact stiffness cannot be so large as to cause instability and nonconvergence. This same strategy is used both in the opposite direction to prevent separation (with bonded or no-separation behaviors) and in the tangential direction to enforce frictional resistance and no-sliding behavior.

The augmented Lagrange method is very similar to the penalty method. The calculated force at the contact detection point(s) is

$F_c=k_c*D_p+ l$ ……...……(eq.12)

in which l is an internally calculated term that augments the penalty-based force calculation. The purpose of the augmentation is to reduce sensitivity to contact stiffness. All things being equal, the augmented Lagrange method should produce less penetration than the pure penalty method, but it might take more iterations to converge. The program-controlled default formulation for contact between flexible bodies is augmented Lagrange.

The optimal value for contact stiffness in these methods is one that generates a converged result in a reasonable number of iterations with a resulting penetration

(or elastic slip in the tangential direction) that is inside acceptable tolerance. Often, such an optimal value will vary as we progress through the load path. To enhance convergence, the program automatically adjusts the stiffness based on the current mean stress of the underlying elements and allowable penetration. We can influence the code-calculated stiffness value by manually defining a multiply factor on the stiffness. Thus, here for our contact we have taken augmented Lagrange.

3.2.3 Contact type

There are basically different type of contact that can be used as per the definition of contact nature between the target and contact surfaces in the connection of bodies namely bonded, frictionless, rough and frictional. Here for cage to ball frictionless definition has been taken into the account. Although whenever any frictional contact is to be taken the value should have upper limit of 0.3 because of the convergence. the values of more than .3 are unable to find the solution directly by using the direct solver and thus even on the successive iterations the solution is unable to converge to a result. In nutshell, our values of friction are always way under the limit of .3 on contrary it is nearly .01 whenever taken.

3.2.4 Contact Stiffness and closure

Taking separately the raceway's groove surface of inner and outer ring as target surface, and taking correspondingly half sphere surfaces of balls as target surface, two contact pairs can be built. It is necessary that to make sure the contact is rigid-flexible contact between rolling element and inner or outer ring, to choose CONTA174 as contact element type which has 8 nodes and quadrilateral include middle node, and to choose TARGE170 as target element type which has 3 nodes without middle-node, to set 0.1 as normal penalty stiffness (FKN) value of each contact pair (if the value is excessive, it will cause some problems which contact analysis doesn't convergent), to set 0.01 as initial contact closure(ICONT) value and 0.003 as friction factor value. After meshing contact element, it is important to check the outer normal direction. To 3D element, the outer normal direction is decided by nodes' number and the right rule. The outer normal direction of contact surface must face to target surface. Otherwise, at the beginning of analysis and calculation, program maybe believes that the contact surface has exceeded

penetration, and it will be difficult to find initial solution, so as to program stop executing. If the direction is wrong, it must be changed by reversing the wrong nodes number (Command: ESURF, REVE or GUI : Main Menu>Preprocessor>Create> Elements>Surf to Surf),or to redefine element normal direction (Command: ENORM or GUI : Main Menu>Preprocessor>Create> Move/Modify> Surf Normal).

3.2.5 Ball to inner race contact

The table below contains the contact settings and properties for the contact between ball to inner race of the deep groove ball bearing

Table 3.4 Contact setting for Ball to inner race

Contact Type	Frictional
Friction coefficient	.03
Trim tolerance	$7.5763e^{-5}$ m (automatic)
Contact Formulation	Augmented Lagrange
Detection method	Automatic
Normal stiffness factor	.1
Interface treatment	Adjust to touch
Initial contact closure	.01

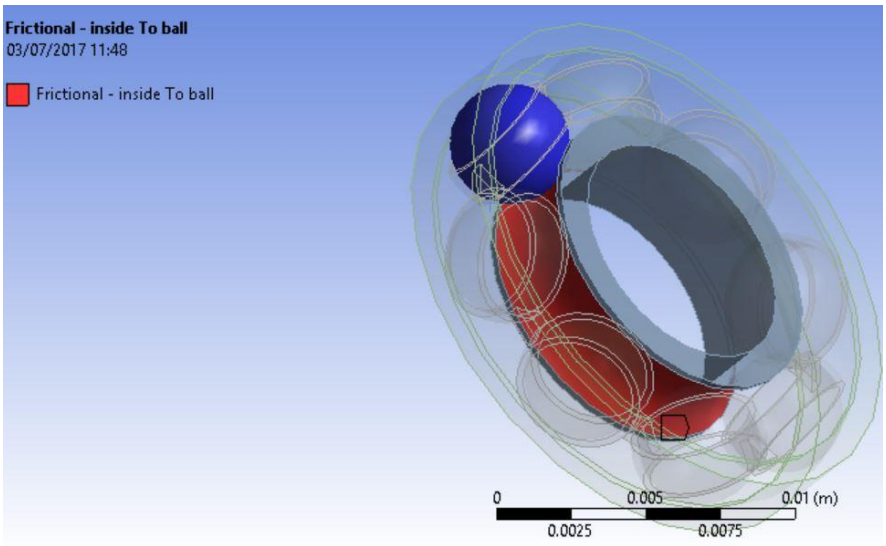

Fig 3.6: Contact between Ball and Inner race

3.2.6 Ball to outer race contact

The ball to outer race contact is defined as frictional contact. The outer race is set as fixed joint. The rolling friction coefficient, contact stiffness, contact formulation and other contact properties are enlisted below in the table.

Table 3.5 Contact setting for Ball to outer race

Contact Type	Frictional
Friction coefficient	.03
Trim tolerance	$7.5763e^{-5}$ m (automatic)
Contact Formulation	Augmented Lagrange
Detection method	Automatic
Normal stiffness factor	.1
Interface treatment	Adjust to touch
Initial contact closure	.01
Outer race joint	Fixed to ground

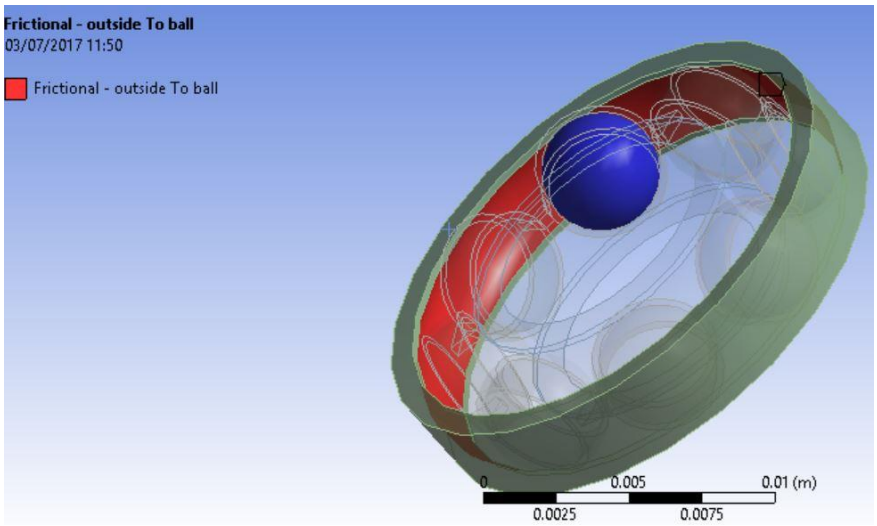

Fig 3.6: Outer Race to Ball contact

3.3 Joint Connections

Joints are type of connection defined to describe the contacts between to bodies where we have to assign relative motions to simulate the constrained motion of the body. Thus, it is highly imperative to define joint as per the boundary conditions. Thus, the final output motion of the system determines the properties of the joints. Here in Ansys we have six joint definitions and namely Fixed, Revolute, translatory, Cylindrical, Slot and Universal.

3.3.1 Inner Race Joint.

Inner race is revolute joint and details are mentioned below in table 3.6

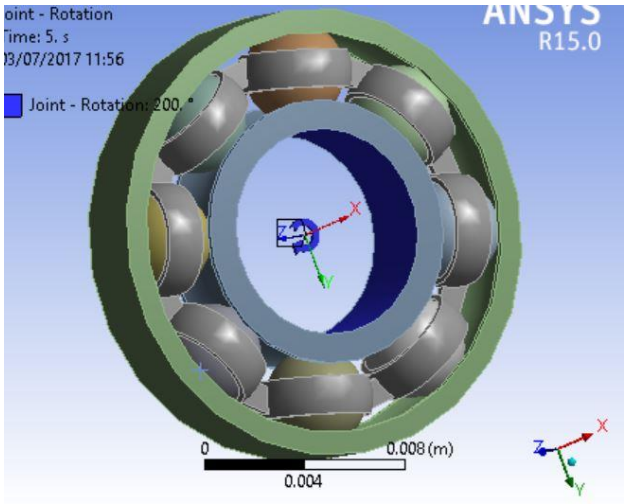

Figure 3.7: Inner race joint

Table 3.6: Inner race joint definition

Connection type		Body to ground
Motion		Revolute Joint
Surfaces		Inside the body surface

3.5.2 Outer Race Joint

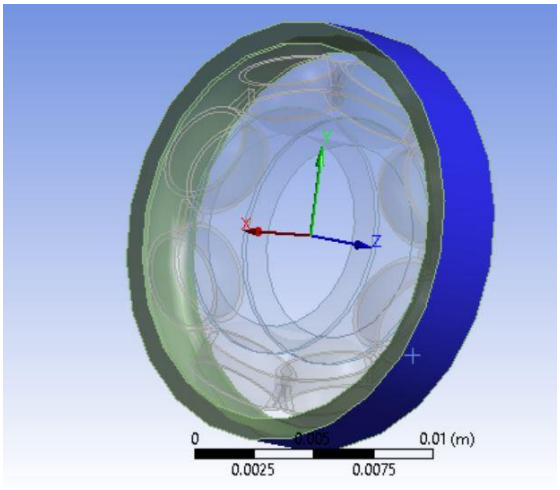

Fig 3.8: Outer race Joint

Table 3.67: Inner race joint definition

Connection type	Body to ground
Motion	Fixed to ground
Surfaces	Inside the body surface

3.4. Mesh Generation

In the Finite element model of deep groove ball Bearing's inner ring, outer ring, rolling element and cage were separately meshed as there was requirement of monitor node to be established below the surface of the defect which should be equally spaced from the both side of the defect. Thus, the outer race was given free meshing along with the cages because they were not the part of system under consideration whereas inner race was meshed using three volume slices and patch conforming in global co-ordinate system was done for symmetric meshing around the defect. The balls were method meshed using automatic control with three degree of refinement.

3.4.1 Meshing of inner race

The first consideration during meshing was to ensure that the volume in the neighborhood of the defect was suitably meshed. This meant that a volume in the defect neighborhood be identified that would be most finely meshed. The defect

only present near the surface of the raceway. Hence it was decided to divide the ring longitudinally, using an arc extruded along the thickness at a depth of 2 mm below the defect. Also, the ring was divided radially by orienting the working plane at 3 and 6 degrees from its global orientation. The area at the intersection of the working plane and the ring was used to divide the volume into sub-volumes. This was done so that a finer mapped mesh could be implemented near the defect.

A free mesh was used for the volume which contained the defect. Free meshing can be used for any kind of solid model. Pyramid-shaped elements were introduced into the tetrahedral mesh for transitioning purposes. Mapped meshing was used to mesh all the other volumes. For mapped meshing, the usage of hexahedral (brick) elements was specified. Mapped meshing can only be used for volumes if they are regular. An equal number of element divisions were specified at the opposite edges so that mapped meshing could be used for the other volumes. This was done by using the LESIZE command. The areas were concatenated using the ACCAT command. Concatenation was necessary because the separate areas were created when the semicircle was extruded to form the raceway in the solid model of the bearing. After setting all these initial controls for the mesh, the next step was the choice of element types to be used for the analysis. For the outer volumes, the element size decided was 2 mm, as a coarser mesh could be used. Three element types had been defined for the analysis: SOLID45, SOLID95 and SOLID92. SOLID45 was used for the outer volumes. SOLID45 is an 8noded element and it has 3 degrees of freedom per node. SOLID95 is a higher order version of SOLID45. Since SOLID95 is 20-noded, a considerably higher amount of time would have been required for computation by ANSYS if it was to be used for the outer volume meshing. Since a high level of accuracy was not required for these elements SOLID45 was used. SOLID95 also has 3 degrees of freedom and it is well suited to model curved boundaries. It was used to mesh the inner volumes. The element size used for these volumes was 0For the defect volume a free mesh was specified and the element size was chosen to be 0.5 mm.. This element has options for tetrahedral, prism and pyramids also. The TCHG command was used for this mesh to convert the 20-node degenerate tetrahedral elements to their 10-node non-degenerate counterparts. This is done so that the computation time and memory usage is lesser as the SOLID92 is 10-noded. The use of free meshing for the defect

volume necessitates that suitable transitioning elements be used at the interface of the mapped and free meshes. Transitional pyramids can be created at the interface of these two meshes. This is required to remove any non-conformities in the mesh. To create transitioning elements, it is required that the elements used are capable of being degenerated into a pyramid shape. SOLID95 is such an element.

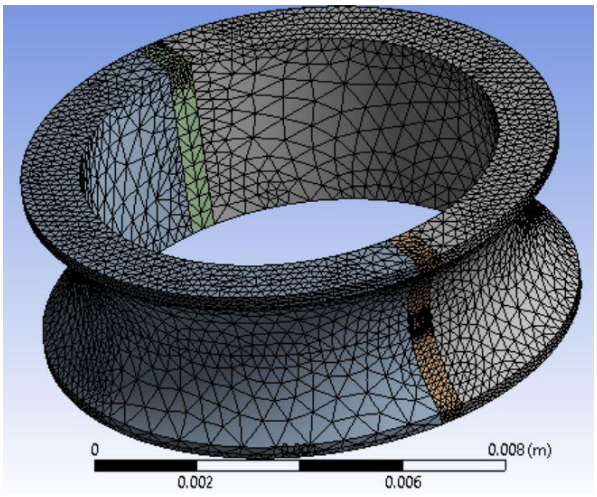

Fig 3.9: Meshed inner race with defect having three volumes

3.4.2 Final mesh results

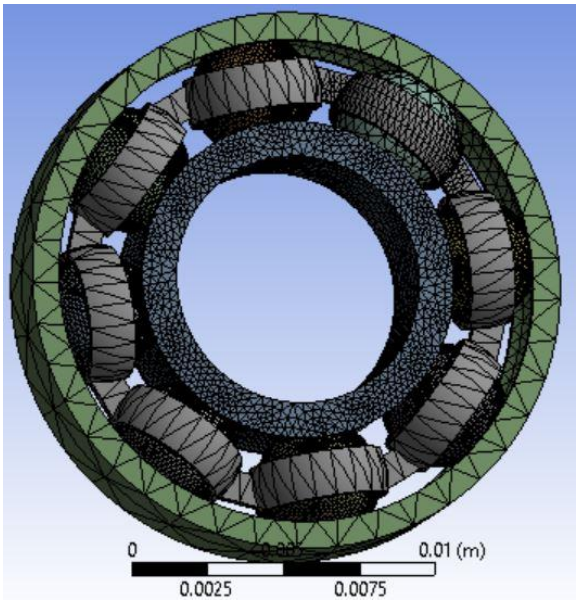

Fig3.10: Meshed structure of deep groove ball bearing assembly

Table 3.8: Mesh Details

Total number of nodes	98056
Total number of elements	42632
Size of mesh for inner race	.2mm
Size of mesh for balls	.6mm
Size of mesh for rest of assembly	1.5 mm

Different mesh sizes from 1 mm to .1 mm were tried for the meshing of inner race and balls but there were no significant changes in the results although computing time increased considerably with decrease in mesh size. The most refined size was selected with trade of between computing time and stability of results along with the limits of system software capabilities.

3.4.3 Mesh sensitivity.

In order to verify the mesh convergence and result independence of the model different mesh size were tried from 1 to .1 mm on the type one defect and then the stability of results was tried to establish. Thus, trade of between result stability and computation time was made. The graph below establishes the mesh convergence results.

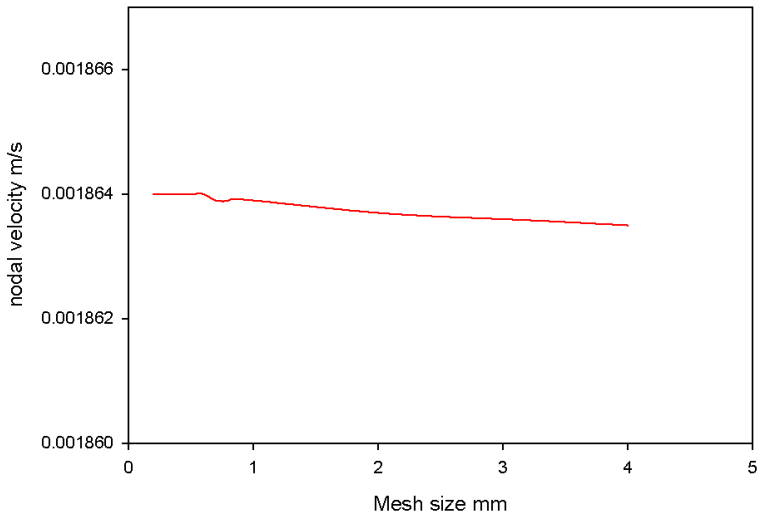

Fig 3.9: Mesh size vs nodal velocity for .1 mm diameter cylindrical defect

3.5 Boundary conditions and loads

We have restrained the all degrees of freedom (DOF) of bearing outer ring's cylinder surface, fixed the displacement of the axial direction（UZ in Cartesian coordinate system）and circle direction(UY in cylindrical coordinate system) of groove surface and bore surface of outer ring, groove surface and cylinder surface of inner ring, ball and cage's nodes in pitch diameter of ball set, added constraint of the axial direction and radial direction(UX in cylindrical coordinate system),and applied radial loads to the lower part's nodes of bore surface in inner ring.

The inner ring revolute joint is given rotational velocity along with the radial load of continuous nature where the load was of bearing load nature and 100N in magnitude for all sizes of defect to maintain an uniformity in order to analyze the effect of changes of shape on the vibrational parameter of the bearing assembly.

Table 3.9: Boundary and Load conditions

Outer race B.C	Fixed
Inner Race B.C	Revolute ,1200 rpm
Inner race bearing load	100 N
Outer race load	0 as no analysis was considered on it

3.6 Analysis setting.

Table 3.10: Analysis setting

Number of steps	5
Number of sub steps	200
Large deflection	On
Mathematical Solver	Newton Raphson
Convergence type	Forced convergence, .05%
Run time	1.2 sec
Energy stabilization	Constant with
Energy dissipation factor	.1

3.7 Structural transient model

A structural transient analysis is a FE analysis that determines the dynamic behavior of a structure or component under arbitrary load. It is an analysis involving time, where apart from mass, stiffness and displacement, inertia and damping of the structure is also taken into account. The governing equation in matrix form for structural transient analysis is given in

$$[m][\ddot{u}] + [c][\dot{u}] + [k][u] = F \ldots\ldots\ldots\ldots\ldots\ldots 11$$

where [m] is the structural mass matrix, [c] is the structural damping matrix, [c] is the structural stiffness matrix, $[\ddot{u}]$ is the nodal acceleration vector, $[\dot{u}]$is the nodal velocity vector, $[u]$ is the nodal displacement vector, is the applied load vector. Nonlinearities, such as large deflections, nonlinear contact, material nonlinearities etc., are possible in a transient analysis. The external force {F} can be time dependent.

CHAPTER 4: RESULTS AND DISCUSSION

In this chapter result of transient structural simulation of each defect is discussed individually to capture the defining parameters and study the variation of these parameter with changes in the size of the defect. The basic features to be studied are the nodal parameters like nodal deformation, total acceleration, nodal directional velocity, total velocity and strain energy absorbed in inner race defect location. Once the individual defects results have been studied then the relative analysis of these parameters is discussed to mark the changes and establish the variations with respect to changes in the size of the defect. These results can be considered to understand the severity and detrimental effects of the defects.

The modelling technique for the localised faults was verified with help of transient analysis of localised fault , where the defect of cylindrical nature of diameter of .5mm and depth of .5mm at 64 N load conditions and inner race rotation at 1200 rpm was simulated on Ansys 15 and nodal acceleration were evaluated .The root mean square acceleration was calculated and cross verified from the results of experimental data presented by S.Tyagi [50] and results were in narrow range of two percent error , where the simulation result was .98 m/s^2 directional acceleration and the actual experimentation result was 1 m/s^2.

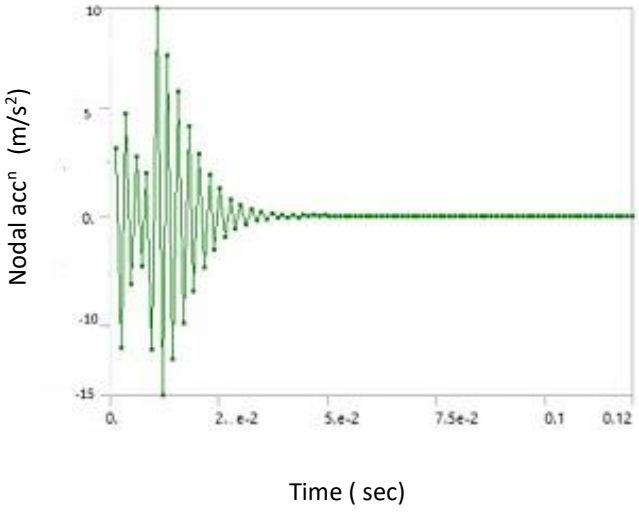

Fig 4.1: Nodal acceleration vs time

4.1 Cylindrical defect with .05 mm diameter

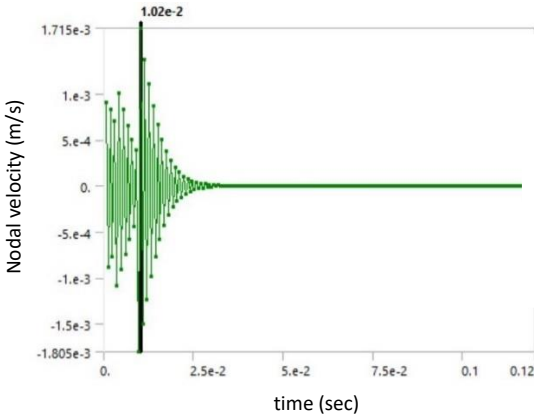

Fig4.2: Directional velocity vs time

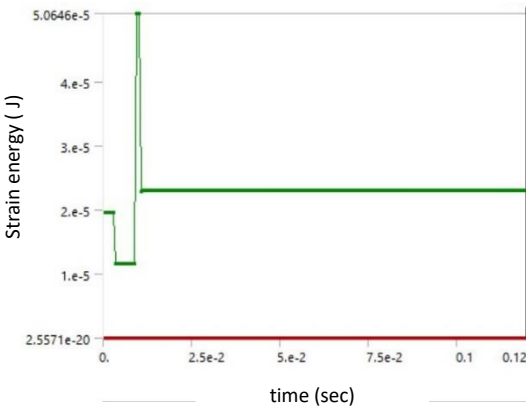

Fig 4.3: Strain energy vs time

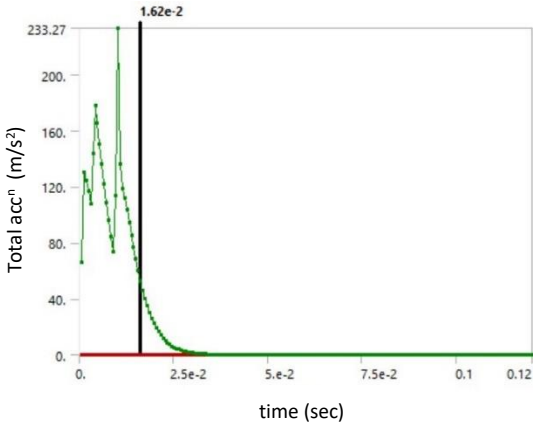

Fig 4.4: Total acceleration vs time

Here for the defect size of .05 mm diameter the maximum amplitude of the nodal velocity of monitor node is 1.8055×10^{-3} m/s and maximum total acceleration absorbed is 233.27m/s^2 whereas directional nodal acceleration is 27.73 m/s$^{2.}$. The maximum strain energy in the inner race due to defect is about 5.0645×10^{-5} J along with nodal deformation of 2.6009×10^{-6} m.

4.2 Cylindrical defect of .1 mm diameter.

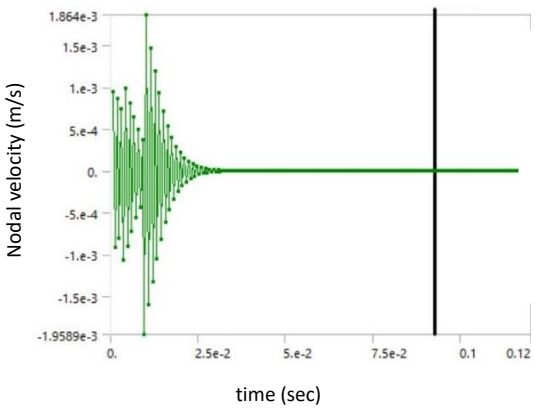

Fig4.5: Directional velocity vs time

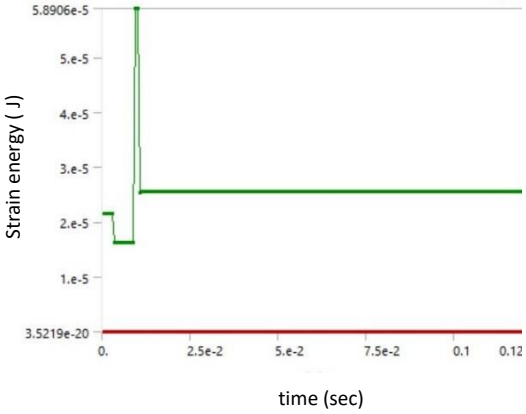

Fig 4.6: Strain energy vs time

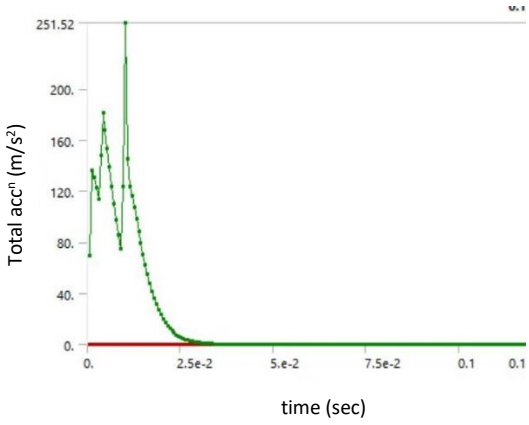

Fig 4.7: Total acceleration vs time

For the defect of .1 mm diameter the maximum amplitude of the nodal velocity of monitor node is 1.864×10^{-3} m/s and maximum total acceleration observed is 233.27m/s^2 whereas directional nodal acceleration remains negligibly changed. The maximum strain energy in the inner race due to defect is about 5.8906×10^{-5} J along with nodal deformation of 2.8085×10^{-6} m.

4.3 Cylindrical Defect of .2 mm diameter

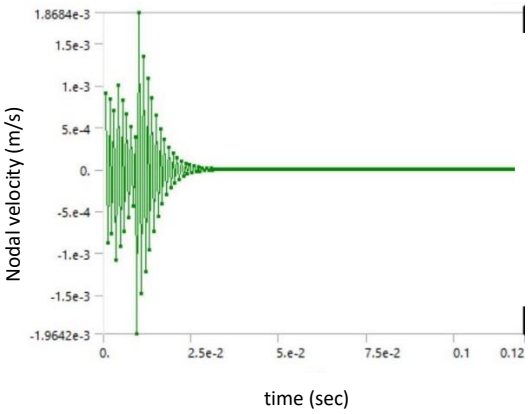

Fig 4.8: Directional velocity vs time

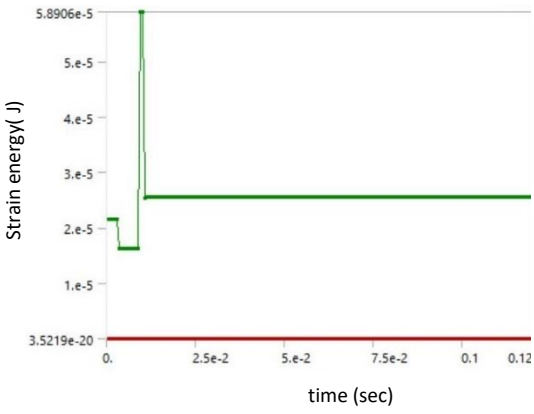

Fig 4.9: Strain energy vs time

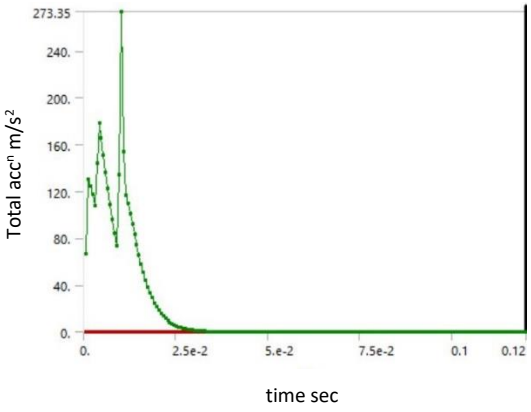

Fig 4.10: Total acceleration vs time

For the defect of .2 mm diameter the maximum amplitude of the nodal velocity of monitor node is 1.9642×10^{-3} m/s and maximum total acceleration observed is 273.27m/s^2 whereas directional nodal acceleration remains negligibly changed. The maximum strain energy in the inner race due to defect is about 6.7805×10^{-5} J along with nodal deformation of 3.014×10^{-6} m. Hence the nodal acceleration effect has almost died out and thus becoming insignificant. So analysing acceleration curve to compare defect size for minor variations is not imperative.

4.4 Cylindrical defect of size .3 mm diameter

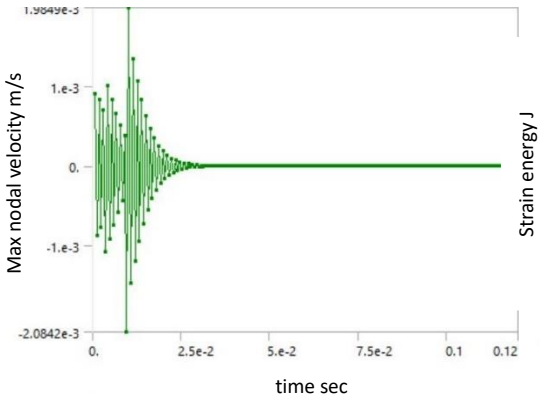

Fig 4.11: Directional velocity vs time

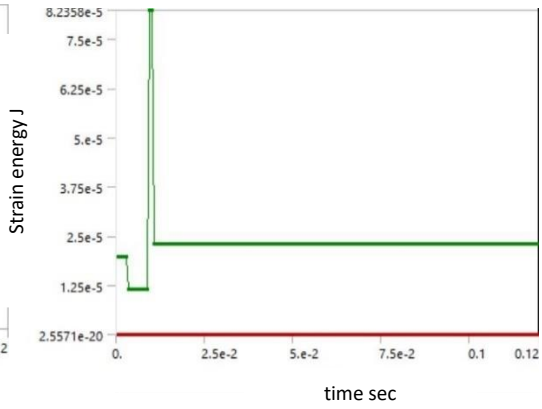

Fig 4.12: Strain energy vs time

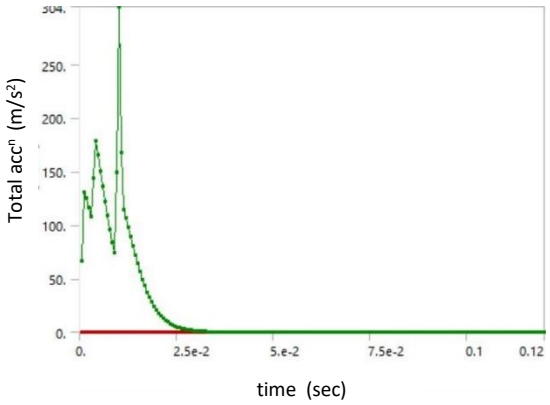

Fig 4.13: Total acceleration vs time

For the defect of .3 mm diameter the maximum amplitude of the nodal velocity of monitor node is 2.0842×10^{-3} m/s and maximum total acceleration observed is 304 m/s^2 whereas directional nodal acceleration remains negligibly changed. The maximum strain energy in the inner race due to defect is about 8.2358×10^{-5} J along with nodal deformation of 3.014×10^{-6} m. Again, from the frequent observation it's clear that nodal velocity, deformation, and total acceleration show the variation of the defect size.

4.5 Square defect of size .4 mm diameter

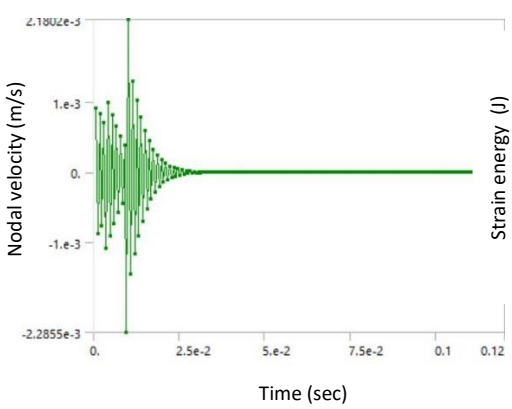

Fig 4.14: Directional velocity vs time

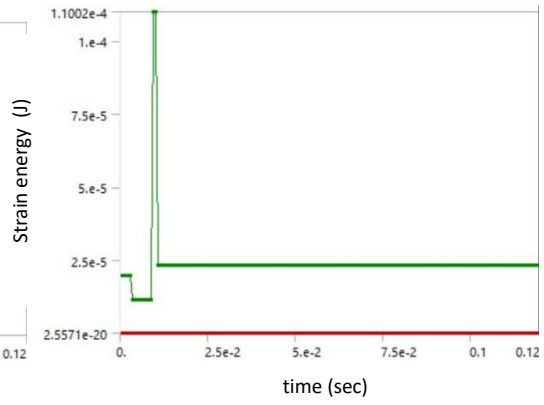

Fig 4.15: Strain energy vs time

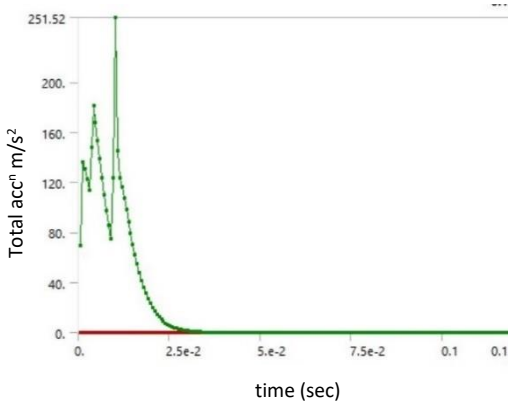

Fig 4.16: Total acceleration vs time

For the defect of .4 mm diameter the maximum amplitude of the nodal velocity of monitor node is 2.1885×10^{-3} m/s and maximum total acceleration observed is 355 m/s^2 whereas directional nodal acceleration remains negligibly changed. The maximum strain energy in the inner race due to defect is about 1.1002×10^{-4} J along with nodal deformation of 3.838×10^{-6} m. Again, from the frequent observation it's clear that nodal velocity, deformation, and total acceleration show the variation of the defect size. Here although there is greater rise in the velocity from compared to previous trend thus signifying that defects after .3mm diameter are really detrimental and sever

4.6 Square defect of size .05×.05mm

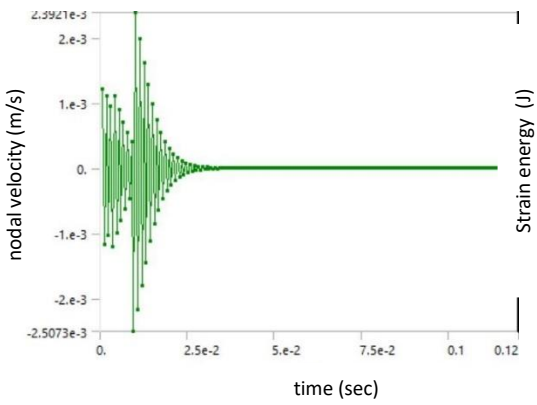

Fig 4.17: Directional velocity vs time

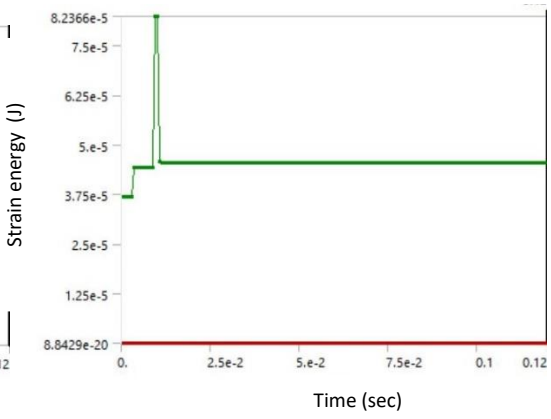

Fig 4.18: Strain energy vs time

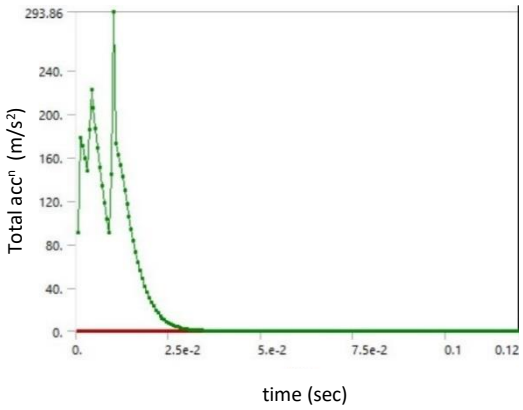

Fig 4.19: Total acceleration vs time

Here for the rectangular defect size of .05mm each side the maximum amplitude of the nodal velocity of monitor node is 2.3921×10^{-3} m/s and maximum total acceleration absorbed is 293m/s^2 whereas directional nodal acceleration is 35.311 m/s$^{2.}$. The maximum strain energy in the inner race due to defect is about 8.2366×10^{-5} J along with nodal deformation of 3.3246×10^{-6} m. There is sudden increase in almost all parameters of nodal response as we move from circular to rectangular.

4.7 Square defect of size .1×.1mm

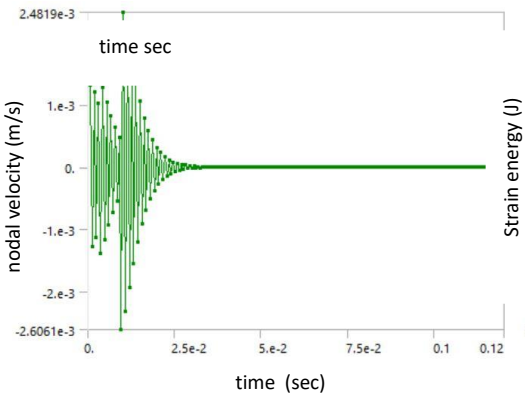

Fig 4.20: Directional velocity vs time

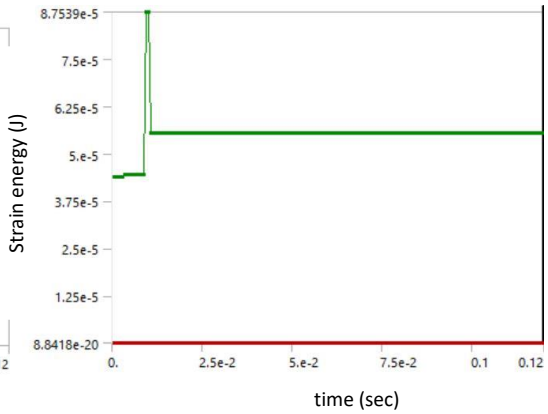

Fig 4.21: Strain energy vs time

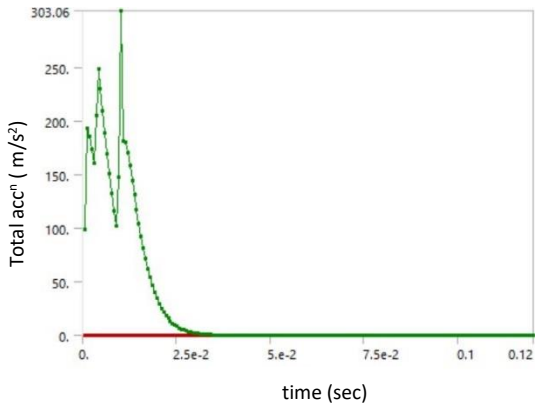

Fig 4.22: Total acceleration vs time

for defect size of .1 mm each side the maximum amplitude of the nodal velocity of monitor node is 2.6061×10^{-3} m/s and maximum total acceleration observed is 303.06 m/s^2 whereas directional nodal acceleration is 35.311 m/s^2 which again has no significant variation. The maximum strain energy in the inner race due to defect is about 8.7539×10^{-5} J along with nodal deformation of 3.4263×10^{-6} m. Thus as defect size increases there is gradual rise in all vibration parameters. Comparatively larger than the all parameters of circular defects.

4.8 Square defect of size .2×.2mm

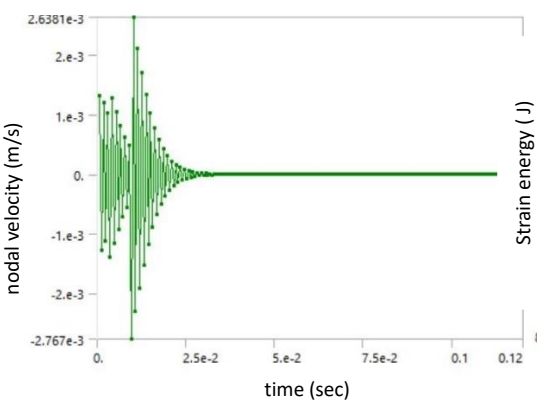

Fig 4.23: Directional velocity vs time

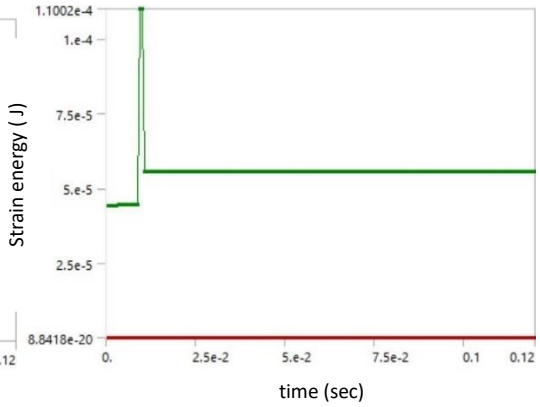

Fig 4.24: Strain energy vs time

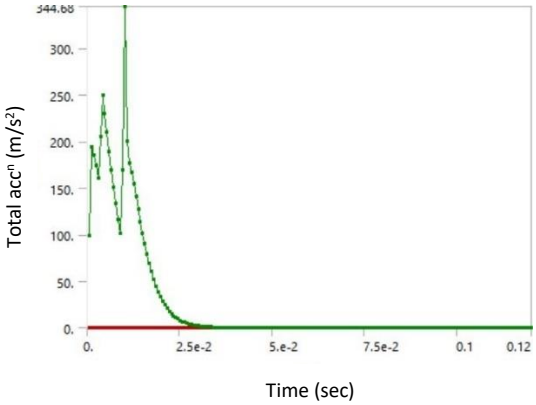

Fig 4.25: Total acceleration vs time

The rectangular defect size of .2mm each side has the maximum amplitude of the nodal velocity of monitor node is 2.6381×10^{-3} m/s and maximum total acceleration observed is 344.68m/s^2 whereas directional nodal acceleration is 35.351 m/s$^{2.}$. The maximum strain energy in the inner race due to defect is about 1.1002×10^{-4} J along with nodal deformation of 3.3246×10^{-6}m.

4.9 Square defect of size .3×.3 mm

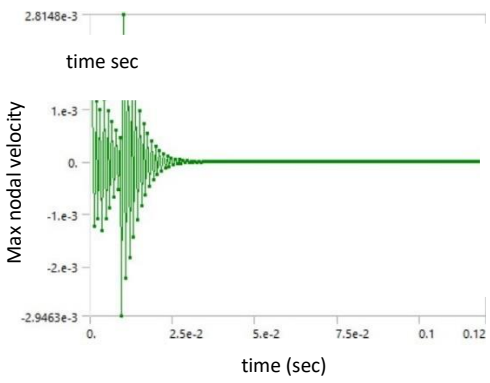

Fig 4.26: Directional velocity vs time

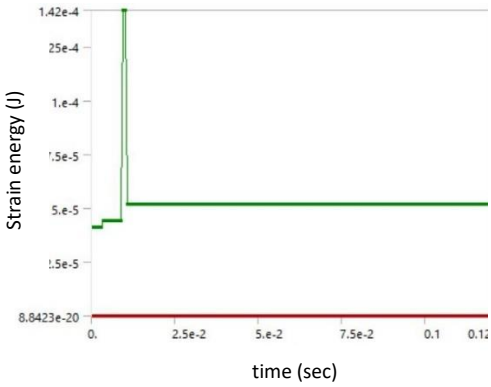

Fig 4.27: Strain energy vs time

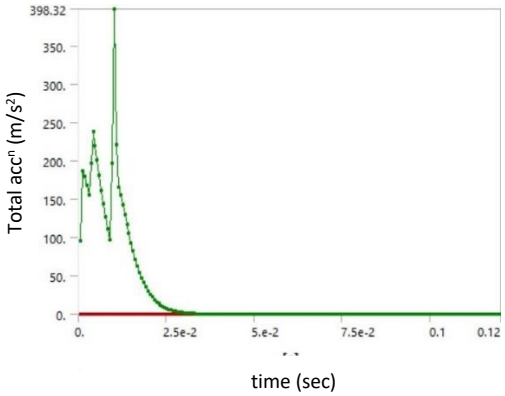

Fig 4.28: Total acceleration vs time

Here for the rectangular defect size of .3mm each side the maximum amplitude of the nodal velocity of monitor node is 2.9463×10^{-3} m/s and maximum total acceleration absorbed is 397.1 m/s^2 whereas directional nodal acceleration is 35.341 m/s$^{2.}$. The maximum strain energy in the inner race due to defect is about 1.4200×10^{-4} J along with nodal deformation of 3.3246×10^{-6} m. There is sudden increase in almost all parameters of nodal response as we move from circular to rectangular.

4.10 Square defect of size .4×.4mm

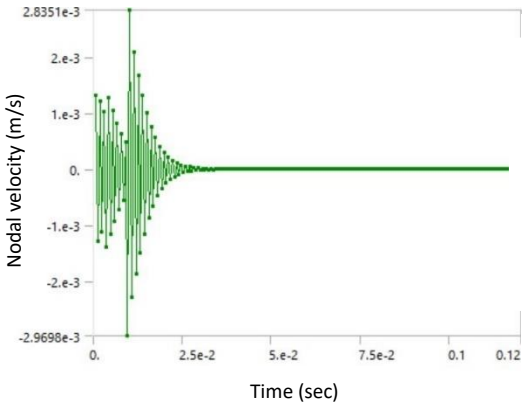

Fig 4.29: Directional velocity vs time

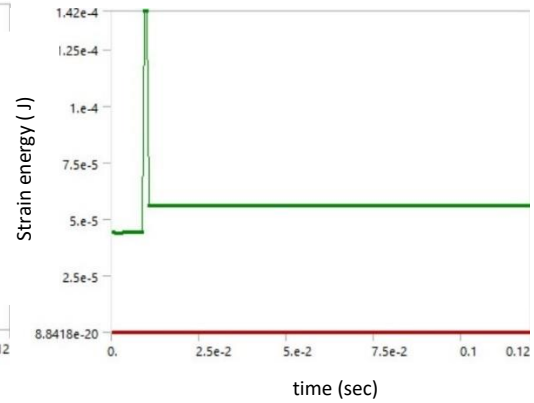

Fig 4.30: Strain energy vs time

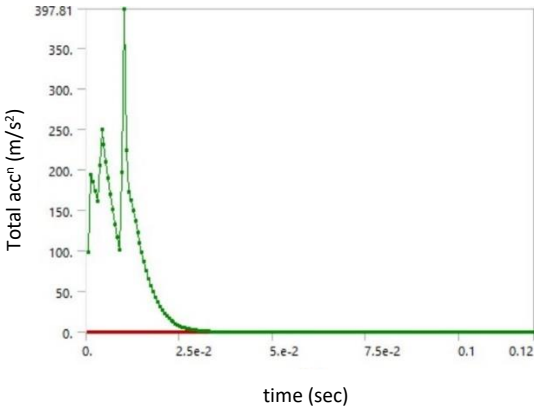

Fig 4.31: Total acceleration vs time

From the simulation results for the rectangular defect size of .4mm each side the maximum amplitude of the nodal velocity of monitor node is 2.9698×10^{-3} m/s and maximum total acceleration absorbed is 398.32 m/s^2 whereas directional nodal acceleration is 35.341 m/s$^{2.}$. The maximum strain energy in the inner race due to defect is about 1.4200×10^{-4} J along with nodal deformation of 4.3525×10^{-6} m. There is sudden increase in almost all parameters of nodal response as we move from circular to rectangular.

4.11 Comparison of cylindrical defects

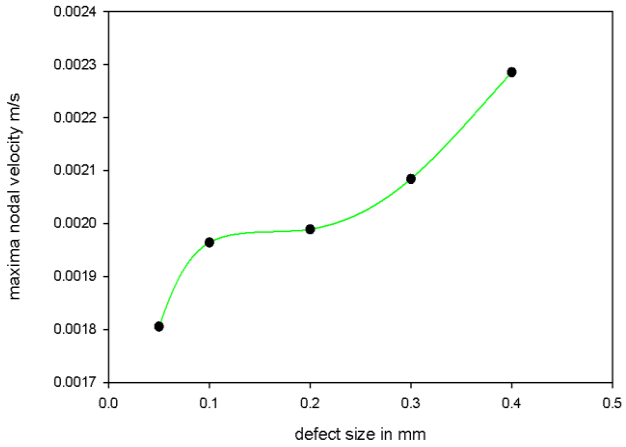

Fig 4.32 .max. nodal velocity vs defect size

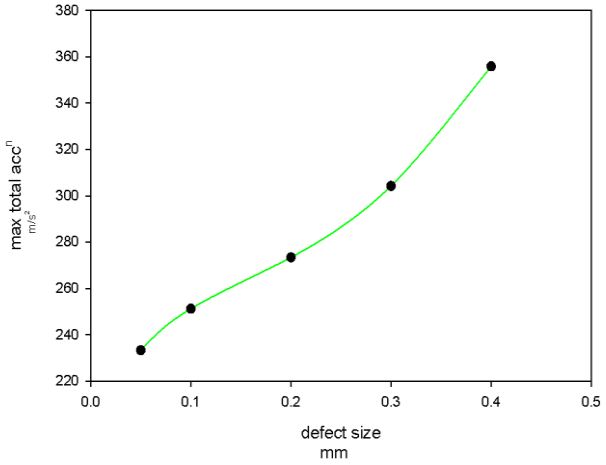

Fig 4.33 max total acceleration v/s defect size

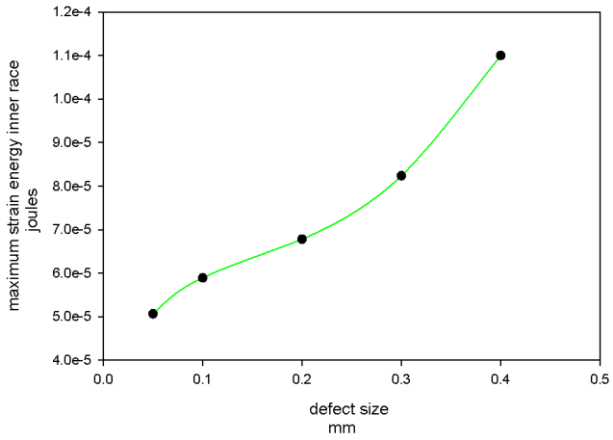

Fig 4.34 max strain energy vs defect size

From these plots, its becomes quite evident the vibrational parameters like nodal velocity, accelerations, directional deformation increase with the gradual increase of the defect size. The strain energy absorbed in the defect region also increase as the defect size increases. From the model, it is also evident that the vibration of system is not that steeply rising for smaller defect as compared to the steep rise when the defect size changes from .2 mm to .3mm and there is even higher detrimental effect of change of defect size from .3 to .4 mm. Thus, using the trends, we can estimate the size of defect depending upon the response region of the particular localised def etc.

4.12 Comparison of rectangular defects.

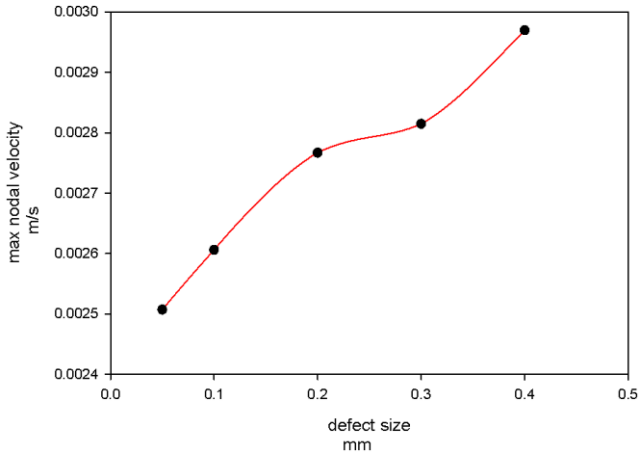

Fig 4.35: nodal velocity vs defect size

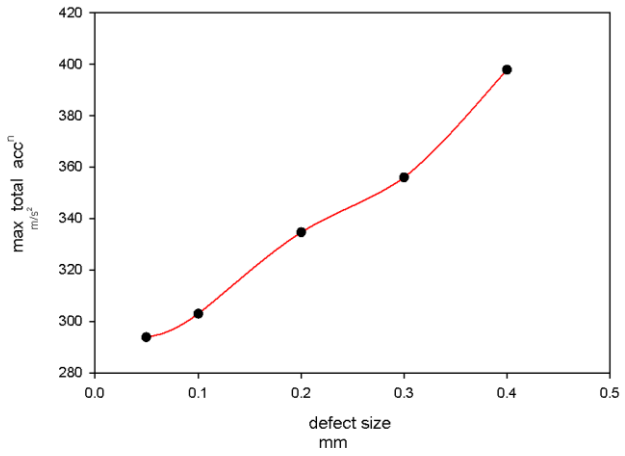

Fig 4.36: Total acceleration vs defect size

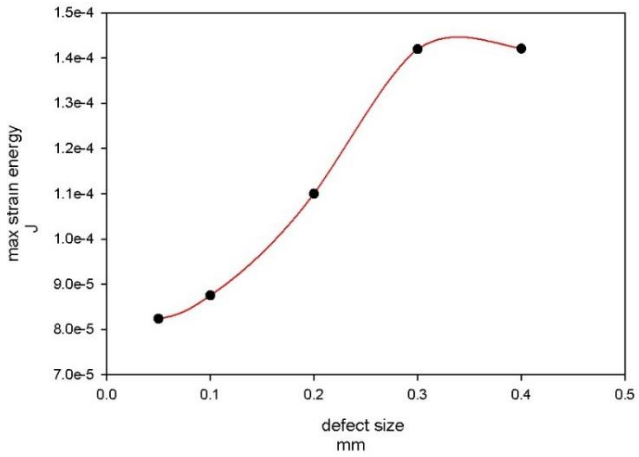

Fig 4.37: Max strain energy in defect

From these comparative charts, it is visible that for rectangular defect the trends of variation of vibration and parameters like maximum velocity amplitude follows the suit of cylindrical defects. Here also after .3 mm defect size there is sudden rise in impact forces leading to very high vibrations which is visible from high magnitude of acceleration and nodal velocity jump and thus detrimental effects of the defects grows in severity in great extent.

4.13 Rectangular vs Cylindrical defects.

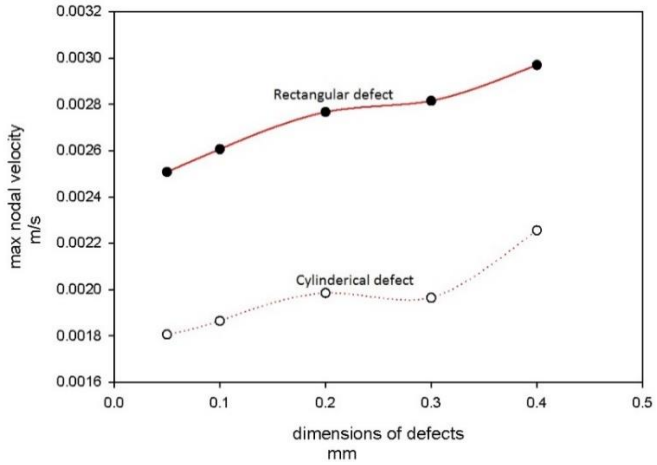

Fig 4.38: Maximum nodal velocity vs defect size

From the above graph, its self-explanatory that the impact generated from the rectangular localised defect is quite high then the cylindrical defect as the amplitude of velocity of vibration is much greater for rectangular defect

CHAPTER 5: CONCLUSION AND FUTURE SCOPE

This project was carried out with aim to implement modern computational design tool to understand the behaviour of rolling element deep groove ball bearing having localised fault and with intent to analyse the effect of varying type of shape and size of localised faults. Thus, from finite element analysis of faulted deep groove ball bearing with the defects located at inner race of the ball bearing, the following conclusions are drawn.

- The rate of increase of impact and vibrations increase in greater magnitude as the size of the defect increases to considerably large size after a range of .2 to .3 mm size of defect despite the shape of the defect.
- Square defect is more detrimental as compared to cylindrical defect as clearly established from the amplitudes of vibrations of the defects.
- Finite element analysis is clearly able to predict the changes in behaviour of vibration response with the change in defect size so FEA could be used for analysing the cause and effect of faults and thereby improving the design.
- Clear trends and curves have been presented that can be used to estimate size and shape of defects and severity of defects for other than the defect size used for FEA in the project.
- The invariance in results after mesh refinement for the defected zone in the inner race has been established.
- The nodal velocities, total acceleration and loss of energy in form of strain energy increases with an increase in the size of the defect.

Future scope

There are further areas to expand this analysis and refine the research work.

- There can be finite element analysis of other defect shapes and defects at different locations in the bearing and even on different types of bearings.
- The FEA models can be practically tested to refine the results and increase the accuracy.
- Signal Processing techniques can be implemented to further analyse these results.
- Instead of modelling ball bearing only, the complete setup of bearing hub, shaft, bearing and other elements can be modelled to improve the results of the analysis.

REFERENCES

1. Cotogno M., Pedrazzi E., Cocconcelli M., Rubini R. , Non-linear Elasto-dynamic Model of Faulty Rolling Elements Bearing ,Proceedings of the 9th International Conference on Rotor Dynamics. Mechanisms and Machine Science, 21 (2015).

2. P Shakya, A K Darpe and M S Kulkarni, Vibration-based fault diagnosis in rolling element bearings: ranking of various time, frequency and time-frequency domain data-based damage identification parameters, The International Journal of Condition Monitoring, 3(2) 2013.

3. Ball and rolling bearing NTN Coperation,2009

4. Nabhan A., Nouby M., Samy A. M. , Mousa, Contact stress distribution of deep groove ball bearing using Abaqus , Journal of the Egyptian society of tribology vol (12) 2015

5. Emil Claesson, modelling of roller bearings in Abaqus ,department of applied mechanics division of material and computational mechanics Chalmers university of technology, 2014.

6. David P. Fleming, J. V. Poplawski, Transient Vibration Prediction for Rotors on Ball Bearings Using Load-Dependent Nonlinear Bearing StiffnessThe International Journal of Condition Monitoring, 3(2) 2013.

7. Shaha Rohit, Vibration Analysis of deep groove ball bearing using Finite Element Analysis, Int. Journal of Engineering Research and Applications, 5(5) 2015.

8. Alfredson RJ, Mathew J., Frequency domain methods for monitoring the condition of rolling element bearings, Mech Engg. Trans, IE Australia ,10(2)1985; 108–12.

9. P. D. McFadden, J. D. Smith, Model for the vibration produced by a single point defect in a rolling element bearing, Journal of Sound and Vibration 96 (1) (1984)69–82.

10. P. D. McFadden, J.D. Smith, Vibration monitoring of rolling element bearings by the high-frequency resonance technique a review, Tribology International 17 (1)(1984)3–10.

11. Sunnersjo C S, Rolling bearing vibrations geometrical imperfections and wear, J Sound Vibr ,98(4) (1985)455–74.

12. Yhland E. A linear theory of vibrations caused by ball bearings with form errors operating at moderate speed. Trans ASME, J Tribol ,(114)(1992)348–59.

13. N. Tandon, A. Choudhary, An analytical model for the prediction of the vibration response of rolling element bearings due to a localized defect, Journal of Sound and Vibration 205 (3) (1997) 275–292.

14. Choudhary A., Tondon N., A theoretical model to predict vibration response rolling bearing to distributed defects under radial load, ASME J. Vibr. Acoust., 12(1998) 214–220.

15. Fawzi M. A. El-Saeidy, Rotating machinery dynamics simulation. I. Rigid systems with ball bearing nonlinearities and outer ring ovality under rotating unbalance excitation, Journal Acoustical Society of America, (2000) 851-860.

16. Akturk N, R Gohar, The effect of ball size variation on vibrations associated with ball-bearings, Proc Inst. Mech Engineers, 212 (J)(1997) 101-110.

17. Brian T. Holm-Hansen Robert X. Gao, Vibration analysis of a sensor integrated ball bearing , Transactions of the ASME, 122 (2000) 384-392.

18. S. Prabhakar, A R Mohanty, A S Sekhar, Application of discrete wavelet transform for detection of ball bearing race faults, Tribology International 35 (2002) 793–800

19. S. A. McInerny and Y. Dai, Basic vibration signal processing for bearing fault detection, IEEE Transactions on Education, 46 (1) (2003), 149-156.

20. M. Amarnath, R. Shrinidhi, A Ramchandra, S B Kandagal, Prediction of defects in antifriction bearings using vibration signal analysis, IE(I) Journal-MC, (2004)88-92.

21. Xinsheng Lou, Kenneth A. Loparo, Bearing fault diagnosis based on wavelet transform and fuzzy inference, Mechanical System and Signal Prpocessing, 18(5) (2004) 1077-1095.

22. V. Purushothama, S. Narayanan, Suryanarayana A. N. Prasad, Multi-fault diagnosis of rolling beraing elements using wavelet analysis and hidden Markov model based fault recognition, NDT&E International 38 (2005) 654–664.

23. R. K. Purohit, K. Purohit, Dynamic analysis of ball bearings with effect of preload and number of balls, Int. Journal of Applied Mechanics and Engineering 11(1) (2006)77–91.

24. A. Choudhary, N. Tandon, Vibration response of rolling element bearings in a rotor bearing system to a local defect under radial load, Journal of Tribology 128 (2)(2006)252–261.

25. Abderrazek Djebala Nouredine Ouelaa Nacer Hamzaoui, Detection of rolling bearing defects using discrete wavelet analysis,Meccanica, Springer.

26. H. Mohamadi Monavar, H. Ahmadi and S. S. Mohtasebi, Prediction of defects in roller bearings using vibration signal analysis, World Applied Science Journal 4 (1) (2008)150-154.

27. Arun Kr. Jalan and A. R. Mohanty, Model based fault diagnosis of a rotor–bearing system for misalignment and unbalance under steady-state condition ,Journal of Sound and Vibration, 2009.

28. G Feng Wang, Yu Bo Li, and Zhi Gao Luo, Fault classification of rolling bearing based on reconstructed phase space and Gaussian mixture model, Journal of Sound and Vibration, 323(3-5), 1077-1089.

29. M. S. Patil, J. Mathew, P. K. Rajendrakumar, S. Desai, A therotical model to predict the effect of localized defect on vibrations associated with ball bearing, International Journal of Mechanical Sciences 52 (2010)1193–1201.

30. F. Cong, J. Chen, G. Dong, M. Pecht, Vibration model of rolling element bearings in a rotor bearing system for fault diagnosis, Journal of Sound and Vibration 332 (2013)2081–2097.

31. S. P. Harsha, K. Sandeep, R. Prakash, Non-linear dynamic behaviours of rolling element bearings due to surface waviness, Journal of Sound and Vibration, 272 (2004) 557–580 .

32. Lin, C-M., Analysis for the Stiffness of Ball Bearings, Master's thesis, Chung Yuan Christian University, Department of Mechanical Engineering, (2002).

33. M. Tadina and M. Boltezar Improved model of a ball bearing for the simulation of vibration signals due to faults during run-up. Journal of Sound and Vibration , 300 (17) (2011)4287-4301.

34. R.K. Upadhyay, Rolling Element Bearing failure analysis: a case study, Elsevier (2013).

35. Weimin Ding, Zhinan Zhang, Fagang Zhao, Vibration response of ball bearings with different defect sizes in the outer raceway: Simulation with a 3-D finite element model, The 14th IFToMM World Congress, Taipei, Taiwan, (2015).

36. Wei Guo, Hongrui Cao, Zhengjia He, and Laihao, Yang Fatigue Life Analysis of Rolling Bearings Based on Quasistatic Modeling Volume 2015 (2015) 982350 .

37. J. Liu, Y. M. Shao, M. J. Zuo, The effects of the shape of localized defect in ball bearings on the vibration waveform, Proceedings of the Institution of Mechanical Engineers, Part K: Journal of Multi-body Dynamics, 227 (3) (2013) .

38. Zhinan Zhang1, Weimin Ding1,2 and Huifang Ma, Local stress analysis of a defective rolling bearing using an explicit dynamic method, Advances in Mechanical Engineering, 8(12)(2016) 1–9 .

39. A.C. McCormick, A.K. Nandi, L.B. Jack, Application of periodic time-varying autoregressive models to the detection of bearing faults, in Proceedings of the Institution of Mechanical Engineers, 212 (6)(1998) 417–428.

40. R. Jiang, J. Chen, G. Dong, T. Liu, W. Xiao, The weak fault diagnosis and condition monitoring of rolling element bearing using minimum entropy deconvolution and envelop spectrum, in Proceedings of the Institution of Mechanical Engineers, 227 (5)(2013)1116–1129.

41. P.W. Tsea, W. Yangb, H.Y. Tama, Machine fault diagnosis through an effective exact wavelet analysis. J. Sound Vib. ,277(2004) 1005–1024.

42. I.E. Alguindigue, A. Loskiewicz-Buczak, R.E. Uhrig, Monitoring and diagnosis of rolling element bearings using artificial neural networks. IEEE Trans. Industr. Electron. 40(2)(1993) 209–217.

43. S. Tyagi, A comparative study of SVM classifiers and artificial neural networks application for rolling element bearing fault diagnosis using wavelet transform pre-processing. J. World Acad. Sci. Eng. Tech. 43(2008) 309–317 .

44. Z. Taha, N.T. Dung, Rolling element bearing fault detection with a single point defect on the outer raceway using finite element analysis. in The 11th Asia Pacific Industrial Engineering and Management Systems Conference, Melaka, Malaysia, (2010) 7–10 .

45. M. Tadina, M.B. Zar, Improved model of a ball bearing for the simulation of vibration signals due to faults during run-up. J. Sound Vib. 300(17), 4287–4301 (2011)

46. L.G. Deshpande, N.M. Sawalhi, R.B. Randall, Bearing fault simulation using finite element model updating and reduction techniques, in Proceedings of the 7th Australasian Congress on Applied Mechanics (ACAM 7), Barton, ACT, Australia, 9–12 (2012) 148-154.

47. T.A. Harris, M.N. Kotzalas, Rolling bearing analysis, 5th edn. edn. (CRC Press, Boca Raton, (2006).

48. A.S. Malhi, Finite element modeling of vibrations caused by a defect in the outer ring of a ball bearing. Project Report finite element method and applications, MIE 605, University of Massachusetts, 2002, pp. 1–6 J. Inst. Eng. India Ser. 95(4) (2014) 309–318 317.

49. H.H. Lee, Finite Element Simulation with ANSYS Workbench 14 Theory Applications and Case Studies (SDC Publications, Kansas, 2012) 25. M. Jovanovic P. Milic , D. Janos evic , G. Petrovic , Accuracy of the FEM analyses in the function of the finite element type selection. Facta Univ. Ser. Mech. Eng. 8(1), (2010).

50. S. Tyagi, S. K. Panigrahi, Ball bearing analysis of fault simulation using finite element method The Institution of Engineers (India), 94(5)(2014).

51. Ansys workbench 15 help and tutorial 2015.

52. SKF bearing official website. http://www.skf.com/.

53. Bearing faults that can be detected with condition monitoring, Meggitt, Wilcoxon research 2011.